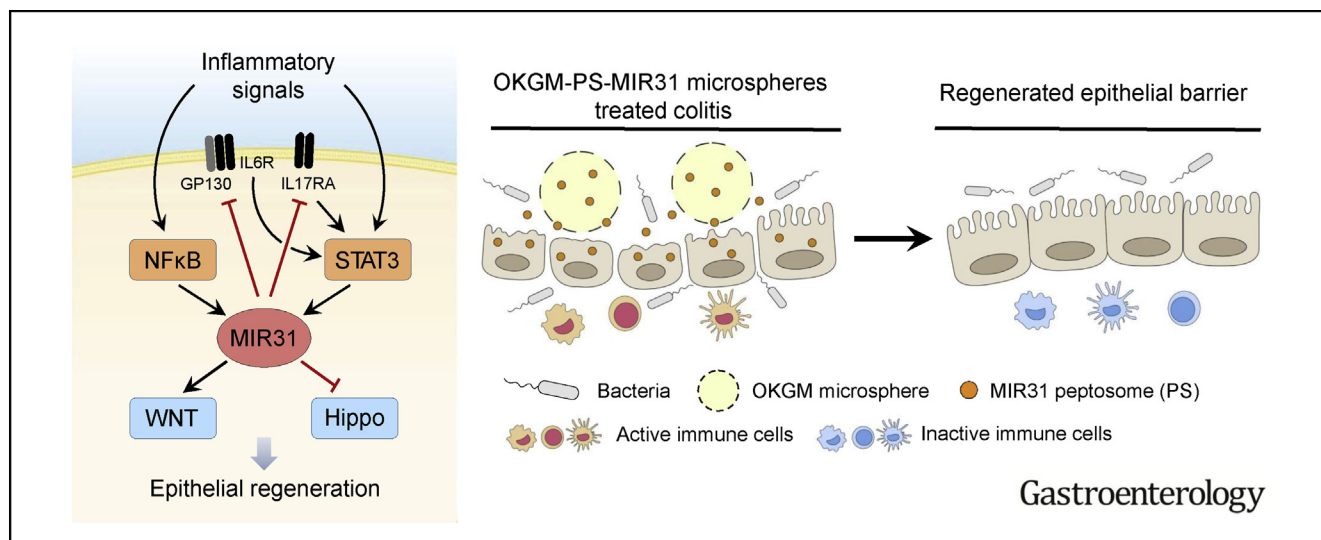




# MicroRNA-31 Reduces Inflammatory Signaling and Promotes Regeneration in Colon Epithelium, and Delivery of Mimics in Microspheres Reduces Colitis in Mice

Yuhua Tian,<sup>1,\*</sup> Jiuzhi Xu,<sup>1,\*</sup> Yuan Li,<sup>2,\*</sup> Ran Zhao,<sup>1</sup> Sujuan Du,<sup>1</sup> Cong Lv,<sup>1</sup> Wei Wu,<sup>3</sup> Ruiqi Liu,<sup>1</sup> Xiaole Sheng,<sup>1</sup> Yongli Song,<sup>1</sup> Xueyun Bi,<sup>1</sup> Guilin Li,<sup>1</sup> Mengzhen Li,<sup>1</sup> Xi Wu,<sup>1</sup> Pengbo Lou,<sup>1</sup> Huiwen You,<sup>4</sup> Wei Cui,<sup>1,5</sup> Jinyue Sun,<sup>6</sup> Jianwei Shuai,<sup>7</sup> Fazheng Ren,<sup>2</sup> Bing Zhang,<sup>8</sup> Mingzhou Guo,<sup>9</sup> Xiaohua Hou,<sup>10</sup> Kaichun Wu,<sup>11</sup> Lixiang Xue,<sup>12</sup> Hongquan Zhang,<sup>13</sup> Maksim V. Plikus,<sup>14</sup> Yingzi Cong,<sup>15</sup> Christopher J. Lengner,<sup>16</sup> Zhanju Liu,<sup>3</sup> and Zhengquan Yu<sup>1</sup>

<sup>1</sup>State Key Laboratories for Agrobiotechnology and Beijing Advanced Innovation Center for Food Nutrition and Human Health and, College of Biological Sciences, China Agricultural University, Beijing, China; <sup>2</sup>Beijing Advanced Innovation Center for Food Nutrition and Human Health and, College of Food Sciences and Nutritional Engineering, China Agricultural University, Beijing, China; <sup>3</sup>Department of Gastroenterology, The Shanghai Tenth People's Hospital, Tongji University, Shanghai, China; <sup>4</sup>School of Pharmaceutical Sciences, Capital Medical University, Beijing, China; <sup>5</sup>Institute of Reproductive and Developmental Biology, Faculty of Medicine, Imperial College London, UK; <sup>6</sup>Institute of Agro-Food Science and Technology, Shandong Academy of Agricultural Sciences, Jinan, China; <sup>7</sup>Department of Physics and State Key Laboratory of Cellular Stress Biology, Innovation Center for Cell Signaling Network, Xiamen University, Xiamen, China; <sup>8</sup>College of Veterinary Medicine, China Agricultural University, Beijing, China; <sup>9</sup>Department of Gastroenterology and Hepatology, Chinese PLA General Hospital, Beijing, China; <sup>10</sup>Division of Gastroenterology, Union Hospital, Tongji Medical College, Huazhong University of Technology and Science, Wuhan, China; <sup>11</sup>Department of Gastroenterology, Xijing Hospital, The Fourth Military Medical University, Xi'an, China; <sup>12</sup>Medical Research Center, Department of Radiation Oncology, Peking University Third Hospital, Beijing, China; <sup>13</sup>Laboratory of Molecular Cell Biology and Tumor Biology, Department of Anatomy, Histology and Embryology, Beijing, China; <sup>14</sup>Department of Developmental and Cell Biology, Sue and Bill Gross Stem Cell Research Center, Center for Complex Biological Systems, University of California, Irvine, Irvine, California; <sup>15</sup>Department of Microbiology and Immunology, University of Texas Medical Branch, Galveston, Texas; and <sup>16</sup>Department of Biomedical Sciences, School of Veterinary Medicine, and Institute for Regenerative Medicine, University of Pennsylvania, Philadelphia, Pennsylvania



**BACKGROUND & AIMS:** Levels of microRNA 31 (MIR31) are increased in intestinal tissues from patients with inflammatory bowel diseases and colitis-associated neoplasias. We investigated the effects of this microRNA on intestinal inflammation by studying mice with colitis. **METHODS:** We obtained colon biopsy samples from 82 patients with ulcerative colitis (UC), 79 patients with Crohn's disease (CD), and 34 healthy individuals (controls) at Shanghai Tenth People's Hospital. MIR31-

knockout mice and mice with conditional disruption of *Mir31* specifically in the intestinal epithelium (MIR31 conditional knockouts) were given dextran sulfate sodium (DSS) or 2,4,6-trinitrobenzene sulfonic acid (TNBS) to induce colitis. We performed chromatin immunoprecipitation and luciferase assays to study proteins that regulate expression of MIR31, including STAT3 and p65, in LOVO colorectal cancer cells and organoids derived from mouse colon cells. Partially hydrolyzed

alpha-lactalbumin was used to generate peptosome nanoparticles, and MIR31 mimics were loaded onto their surface using electrostatic adsorption. Peptosome–MIR31 mimic particles were encapsulated into oxidized konjac glucomannan (OKGM) microspheres, which were administered by enema into the large intestines of mice with DSS-induced colitis. Intestinal tissues were collected and analyzed by histology and immunohistochemistry. **RESULTS:** Levels of MIR31 were increased in inflamed mucosa from patients with CD or UC, and from mice with colitis, compared with controls. STAT3 and nuclear factor- $\kappa$ B activated transcription of MIR31 in colorectal cancer cells and organoids in response to tumor necrosis factor and interleukin (IL)6. MIR31-knockout and conditional-knockout mice developed more severe colitis in response to DSS and TNBS, with increased immune responses, compared with control mice. MIR31 bound to 3' untranslated regions of *I17ra* and *I17r* messenger RNAs (RNAs) (which encode receptors for the inflammatory cytokines IL17 and IL7) and *I6st* mRNA (which encodes GP130, a cytokine signaling protein). These mRNAs and proteins were greater in MIR31-knockout mice with colitis, compared with control mice; MIR31 and MIR31 mimics inhibited their expression. MIR31 also promoted epithelial regeneration by regulating the WNT and Hippo signaling pathways. OKGM peptosome–MIR31 mimic microspheres localized to colonic epithelial cells in mice with colitis; they reduced the inflammatory response, increased body weight and colon length, and promoted epithelial cell proliferation. **CONCLUSIONS:** MIR31, increased in colon tissues from patients with CD or UC, reduces the inflammatory response in colon epithelium of mice by preventing expression of inflammatory cytokine receptors (IL7R and IL17RA) and signaling proteins (GP130). MIR31 also regulates the WNT and Hippo signaling pathways to promote epithelial regeneration following injury. OKGM peptosome–MIR31 microspheres localize to the colon epithelium of mice to reduce features of colitis. Transcript Profiling: GSE123556

**Keywords:** IBD; Nanoparticle Delivery System; Post-transcriptional Processing; Gene Regulation.

Inflammatory bowel disease (IBD), including ulcerative colitis (UC) and Crohn's disease (CD), encompasses chronic inflammatory diseases characterized by the sub-mucosal accumulation of inflammatory cells and damage to the epithelial layer.<sup>1</sup> During inflammatory reaction, immune cells involving both innate and adaptive immunity secrete proinflammatory cytokines to promote mucosal immunity, consequently removing pathogen-infected cells.<sup>2</sup> Increasing evidence indicates that epithelial cells play a central role in regulating the immune response in the intestines. In response to inflammatory signals, intestinal epithelial cells (IECs) are exposed to many proinflammatory cytokines secreted by immune and stromal cells, and respond to these signals through numerous cell surface receptors, including interleukin (IL)17RA, GP130, and IL7R.<sup>2</sup> IECs themselves also produce a variety of cytokines to modulate intestinal mucosal immunity. For example, when IL6 binds to its coreceptor GP130 to activate the signal transduction and activator of transcription 3 (STAT3) signaling pathway in

## WHAT YOU NEED TO KNOW

### BACKGROUND AND CONTEXT

Levels of microRNA 31 (MIR31) are increased in intestinal tissues from patients with inflammatory bowel diseases and colitis-associated neoplasias.

### NEW FINDINGS

MIR31, which is increased in colon tissues from patients with Crohn's disease or ulcerative colitis, reduces the inflammatory response in colon epithelium of mice by preventing expression of inflammatory cytokine receptors and signaling proteins. MIR31 also regulates the WNT and Hippo signaling pathways to promote epithelial regeneration following injury.

### LIMITATIONS

The therapeutic efficacy of MIR31 mimic microspheres in treating human inflammatory bowel diseases was not examined.

### IMPACT

Strategies to deliver MIR31 to inflamed colonic epithelium via microspheres might be developed for treatment of patients with inflammatory bowel diseases.

IECs, it results in the production of proinflammatory cytokines.<sup>3</sup> In addition, epithelial IL17RA has been implicated in controlling autoimmune inflammation.<sup>4</sup> Thus, the cytokines secreted by both epithelial cells and immune cells are involved in a cellular cross-talk that promotes the activation of mucosal immunity. In addition to modulation of the immune system, epithelial cells play a fundamental and intrinsic role against IBD (ie, restoration and maintenance of barrier function). Multiple signaling pathways, including the WNT, Notch, and Hippo pathways, have been identified to promote epithelial regeneration.<sup>5–7</sup> Although some cytokines appear to concomitantly promote both mucosal immunity and epithelial regeneration,<sup>8</sup> it is clear that the immunomodulatory and regenerative functions of the epithelium can be controlled by distinct signals<sup>9,10</sup>; however, it is still not fully understood how the signals are coordinated in controlling the immune response and epithelial regeneration. Therefore, elucidating the precise molecular mechanisms coordinating inflammation and epithelial regeneration is fundamental for understanding IBD, and will provide avenues for therapeutic development.

\* Authors share co-first authorship.

**Abbreviations used in this paper:**  $\alpha$ -La,  $\alpha$ -lactalbumin; CD, Crohn's disease; cKO, conditional knockout; DSS, dextran sulfate sodium; IBD, inflammatory bowel disease; IECs, intestinal epithelial cells; IL, interleukin; KO, knockout; Mal, maleimide; MIR 31, microRNA 31; NF- $\kappa$ B, nuclear factor  $\kappa$ B; OKGM, oxidized konjac glucomannan; PS, peptosome; STAT3, signal transduction and activator of transcription 3; TNBS, 2,4,6-trinitrobenzene sulfonic acid; TNF, tumor necrosis factor; UC, ulcerative colitis; WT, wild type; 3'UTR, 3' untranslated region.

 Most current article

© 2019 by the AGA Institute  
0016-5085/\$36.00

<https://doi.org/10.1053/j.gastro.2019.02.023>

Increasing evidence indicates that many microRNAs are altered in IBD, and play important roles in regulating the pathogenesis of IBD through the direct suppression of different functional targets.<sup>11,12</sup> Among them, microRNA 31 (MIR31) is increased in IBD,<sup>13,14</sup> and further up-regulated during the progression of inflammation-associated intestinal neoplasia.<sup>15</sup> Recently, we identified MIR31 as an important modulator of intestinal stem cells, promoting epithelial regeneration in response to DNA damaging injury by activating dormant stem cells that survive high-dose radiation exposure.<sup>16</sup> Furthermore, *in vitro* evidence indicates that MIR31 directly targets IL25 to regulate Th1/Th17 cell-mediated mucosal inflammation in colitis,<sup>17</sup> suggesting a critical role of MIR31 in inflammation. Therefore, we aimed to determine how MIR31 coordinates epithelial regeneration and the immune response *in vivo* in mouse models of IBD.

Our results showed that MIR31 was up-regulated in IBD tissues, directly via the nuclear factor (NF)- $\kappa$ B and STAT3 signaling pathways. In turn, MIR31 attenuated the inflammatory response by directly targeting *Il17ra*, *Il7r*, and *Il6st* (encoding Gp130) within the colonic epithelium, while concomitantly promoting epithelial cell proliferation by regulating both WNT and Hippo signaling pathways. Moreover, we developed an MIR31-based microsphere delivery system that can suppress the inflammatory response and promote epithelial regeneration in experimental colitis, suggesting a viable therapeutic approach for the treatment of IBD.

## Materials and Methods

Note: The full Materials and Methods section is included in the [supplementary documents](#).

### Subjects

All patients with IBD were recruited from the Department of Gastroenterology, Shanghai Tenth People's Hospital of Tongji University (Shanghai, China) from January 2017 to November 2018. The diagnosis of IBD was based on conventional clinical, radiological, and endoscopic features and was finally confirmed by histological examination of intestinal biopsies. Inflamed ileal and/or colonic tissues were collected from 79 patients with CD and 82 patients with UC who underwent endoscopy. Biopsies were collected from sites of active inflammation adjacent to ulcerations or normal mucosa according to the experimental requirement. Macroscopically and microscopically unaffected ileal and/or colonic mucosa samples were also collected from 34 healthy controls. Clinical characteristics of patients with IBD and controls are shown in [Supplementary Table 1](#). This study was approved by the Institutional Review Board for Clinical Research of the Shanghai Tenth People's Hospital of Tongji University and the methods were carried out in accordance with the approved guidelines. Informed consent was obtained from all subjects.

### Mouse Strains

The *MIR31*<sup>-/-</sup> and MIR31 floxed mice have been previously described.<sup>16,18</sup> *Villin-Cre* mice were purchased from National

Resource Center of Model Mice (stock number: T000142). *Axin2-LacZ* mice were obtained from the Yi Zeng Laboratory (Shanghai Institute of Biochemistry and Cell Biology). All mouse experimental procedures and protocols were evaluated and authorized by the Regulations of Beijing Laboratory Animal Management and were strictly in accordance with the guidelines of the Institutional Animal Care and Use Committee of China Agricultural University (approval number: SKLAB-2011-04-03).

### Statistical Analysis

Most statistical analyses were performed in at least triplicate, and the means obtained were used for independent *t*-tests. Means and standard deviations from at least 3 independent experiments are presented in all graphs. Asterisks denote statistical significance (\**P* < .05; \*\**P* < .01; \*\*\**P* < .001). Statistical analysis was performed using 1-way analysis of variance for [Figure 1A](#). Pearson's correlation analysis was performed for [Figure 1C](#) and [D](#).

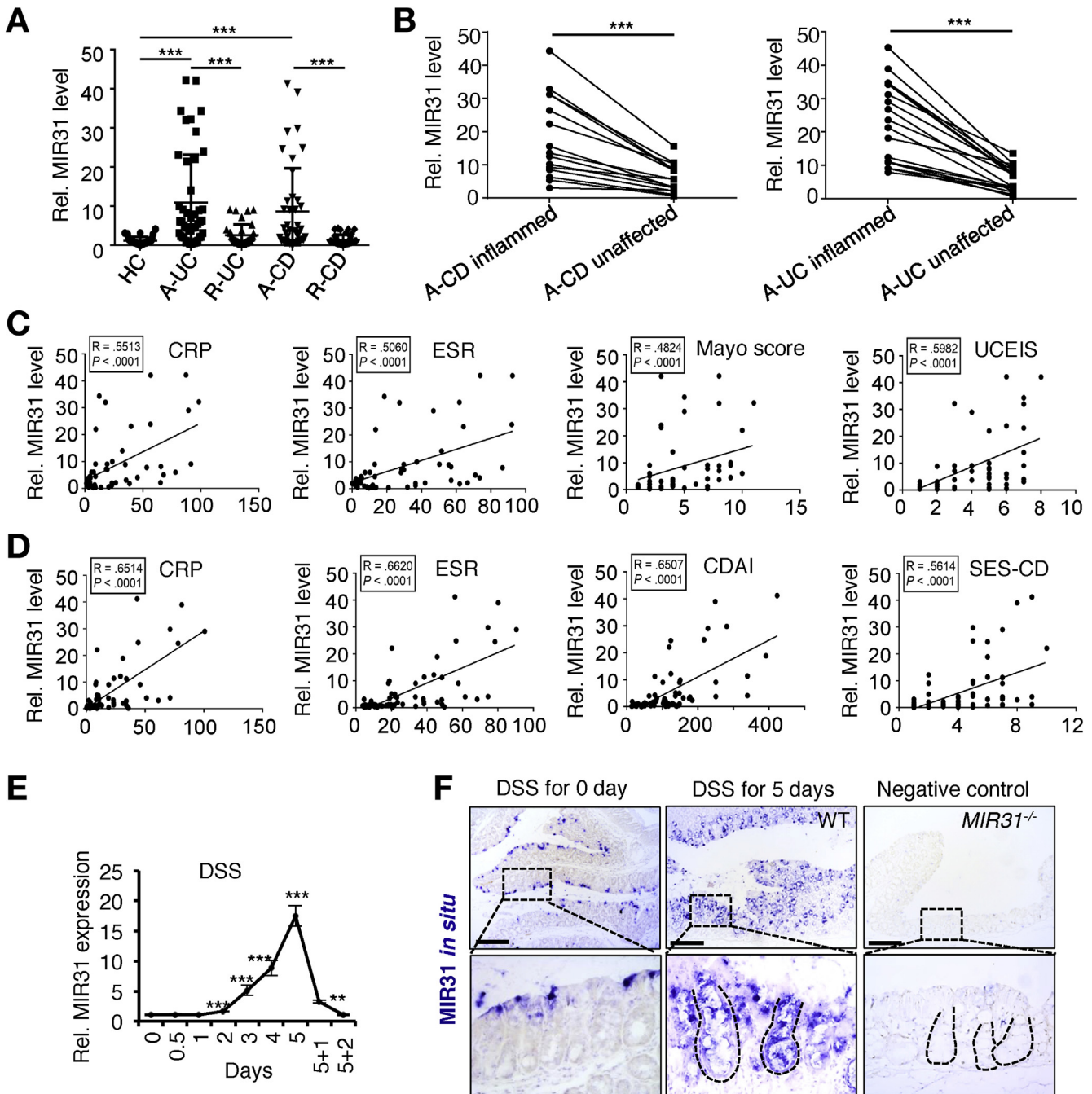
## Results

### *MIR31 Is Increased in Inflamed Mucosa of IBD and Regulated by the STAT3 and NF- $\kappa$ B Signaling Pathways*

To determine the role of MIR31 in the pathogenesis of IBD, we examined MIR31 expression in human samples from patients with active UC or CD, as well as disease in remission. We found that MIR31 was dramatically up-regulated in the inflamed mucosa of patients with active UC or CD, and reduced to the levels similar to unaffected controls in patients in remission ([Figure 1A](#)). Compared with unaffected mucosa, MIR31 was significantly up-regulated in the inflamed mucosa from the same patients ([Figure 1B](#)). *In situ* hybridization also showed that MIR31 expression was elevated in inflamed mucosa from both patients with CD (*n* = 10) and patients with UC (*n* = 10) relative to unaffected controls ([Supplementary Figure 1A](#)). The levels of MIR31 expression in inflamed intestinal mucosa were positively correlated to the values of C-reactive protein, erythrocyte sedimentation rate, Mayo score, and UC endoscopic index of severity in patients with UC, and the values of C-reactive protein, erythrocyte sedimentation rate, CD activity index, and simple endoscopic score for CD in patients with CD, respectively ([Figure 1C](#) and [D](#)). We next used dextran sulfate sodium (DSS) in drinking water to induce experimental colitis in mice. We observed a dramatic up-regulation of MIR31 in inflamed colon following DSS treatment ([Figure 1E](#) and [F](#)). Two days after DSS withdrawal following a 5-day pulse, MIR31 expression rapidly decreased, returning to the pretreatment baseline ([Figure 1E](#)). We found that MIR31 expressed predominantly in colonic epithelial cells; however, DSS-induced MIR31 expression was also observed in leukocytes and stromal cells ([Supplementary Figure 1B](#)). We previously identified 1 STAT3 and 2 NF- $\kappa$ B binding sites in the promoter of MIR31 ([Supplementary Figure 1C](#)).<sup>16,18</sup> Thus, we investigated whether the induction of MIR31 was due to the activation of

these signaling pathways. In response to DSS treatment, both STAT3 and NF- $\kappa$ B pathways were activated in the colon (Supplementary Figure 1D). To test whether the STAT3 and NF- $\kappa$ B activities induce MIR31 expression, we treated LOVO colorectal cancer cells with IL6 and tumor necrosis factor (TNF) to stimulate STAT3 and NF- $\kappa$ B signaling, respectively. We found that TNF induced MIR31 expression concomitant with NF- $\kappa$ B pathway activation (Supplementary Figure 1E). Similarly, MIR31 expression was induced in response to IL6 treatment concomitant with STAT3 pathway activation (Supplementary Figure 1F). Conversely, knockdown of STAT3 with small interfering RNA suppressed MIR31

expression (Supplementary Figure 1G). To eliminate the possibility that these effects were influenced by the malignant LOVO cells, we also verified that MIR31 was induced in primary mouse colon organoids in response to TNF and IL6 (Supplementary Figure 1H). Luciferase reporter assays revealed that mutation of p-STAT3 or p65 (the transcriptional effector of NF- $\kappa$ B signaling) binding sites blocked the reporter activity of MIR31 (Supplementary Figure 1I), and chromatin immunoprecipitation further proved that p-STAT3 and p65 interact with their binding sites in the MIR31 promoter (Supplementary Figure 1J). Taken together, these findings indicate that the STAT3 and NF- $\kappa$ B



signaling pathways directly mediate the induction of MIR31 in IBD.

### Loss of MIR31 Exacerbates the Inflammatory Response and Delays Epithelial Regeneration

Next, we examined the effect of MIR31 loss on the colon by using both MIR31 germline knockout (KO) and *Villin-Cre*-driven colonic epithelial conditional KO (cKO) mice (Supplementary Figure 2A). We have previously shown that these mice have no apparent gross phenotypes.<sup>16</sup> The colon length was not significantly altered in MIR31 KO and cKO mice as compared with the controls (Supplementary Figure 2B). No significant difference was found in cell proliferation in crypts, apoptosis at the tip, or the number of Goblet cells between wild-type (WT) and KO mice (Supplementary Figure 2C–I).

To further assess the role of MIR31 in colitis, we induced colitis in both WT and MIR31 KO mice by administering DSS in drinking water. DSS was administered for 5 days, followed by 3 days of recovery. After 4 days of DSS treatment, *MIR31*<sup>-/-</sup> mice exhibited considerably more weight loss than WT mice and showed no weight recovery on termination of the treatment (Figure 2A). This was accompanied by a lower survival rate (Figure 2B), shorter colon length (Figure 2C and D), larger spleens (Figure 2C and D), and higher clinical disease scores (Figure 2E) compared with controls. A time-course analysis showed a severe inflammatory response on DSS treatment and an impaired regenerative response after DSS removal in *MIR31*<sup>-/-</sup> mice (Figure 2F). A reduction in proliferative epithelial cells was found in *MIR31*<sup>-/-</sup> mice (Figure 2G), which was further confirmed by bromodeoxyuridine incorporation assay (Supplementary Figure 3A and C). In contrast, the number of apoptotic cells was markedly increased in the colonic epithelium of *MIR31*<sup>-/-</sup> mice (Supplementary Figure 3B and D). There was also a decrease in the number of Goblet cells in *MIR31*<sup>-/-</sup> colonic epithelium upon DSS treatment (Supplementary Figure 3E). Furthermore, permeability assays revealed reduced barrier function in the colonic

epithelium of *MIR31*<sup>-/-</sup> mice following 3 days of DSS treatment (Supplementary Figure 3F). Similar consequences of MIR31 deletion were also found in another model of 2,4,6-trinitrobenzene sulfonic acid (TNBS)-induced colitis in mice (Supplementary Figure 4A–G). In contrast, MIR31 overexpression inhibited colitis in TNBS-induced murine colitis (Supplementary Figure 5A–F). Furthermore, MIR31 deletion also resulted in exacerbated inflammatory response in TNBS-induced chronic colitis in mice (Supplementary Figure 6A–E). Taken together, our results demonstrate that MIR31 plays a key role in suppressing the inflammatory response and promoting epithelial regeneration in colitis.

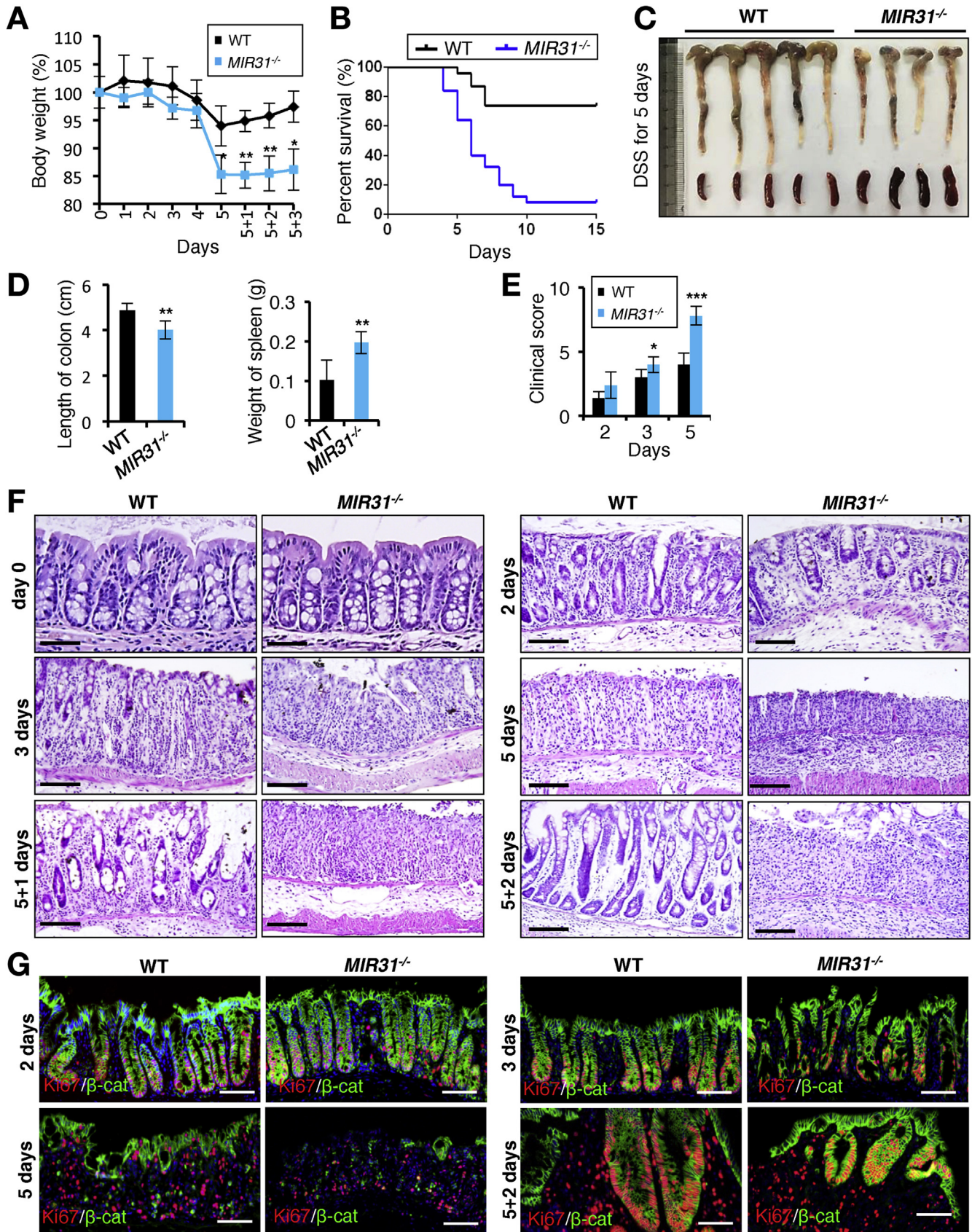
We next characterized the enhanced immune response in *MIR31*<sup>-/-</sup> mice after DSS treatment. We found increased numbers of leukocytes and macrophages (Figure 3A and B), increased levels of proinflammatory cytokines and inflammasome components, and decreased levels of the inflammatory suppressor IL10 in *MIR31*<sup>-/-</sup> mice on DSS treatment (Figure 3C–G). Consistently, the proinflammatory NF- $\kappa$ B and STAT3 signaling pathways were overactivated in *MIR31*<sup>-/-</sup> mice (Figure 3H and I). Our findings demonstrate that loss of MIR31 results in a hyperactive immune reaction to DSS treatment.

To test whether the phenotypes observed on MIR31 loss were of epithelial origin, we examined the phenotypes of *Villin-Cre;MIR31*<sup>fl/fl</sup> (cKO) mice on DSS treatment. Similar to the *MIR31*<sup>-/-</sup> mice, cKO mice exhibited enhanced immune response and delayed regeneration in response to DSS treatment (Supplementary Figure 7A–F and Supplementary Figure 8A–D), implying an epithelial cell-autonomous role of MIR31.

### MIR31 Directly Suppresses the Expression of Il6st (Encoding GP130), Il7r, and Il17ra Within Colonic Epithelium

To understand how MIR31 suppresses the immune response in the colonic epithelium, we analyzed MIR31 binding sites in 3' untranslated regions (3'UTRs) of

**Figure 1.** MIR31 expression is up-regulated in human IBD and mouse colitis. (A) MIR31 expression was significantly increased in inflamed mucosa of patients with IBD. Total RNA was isolated from intestinal biopsies of healthy controls (HCs, n = 34), inflamed mucosa of patients with active UC (A-UC, n = 45) or active CD (A-CD, n = 41), and intestinal mucosa of patients with UC with remission (R-UC, n = 37) or patients with CD with remission (R-CD, n = 38). MIR31 expression was analyzed by quantitative reverse-transcriptase polymerase chain reaction (qRT-PCR) and normalized to U6. \*\*\**P* < .001. Statistical analysis was performed using 1-way analysis of variance. (B) Expression of MIR31 in inflamed and unaffected mucosa from the same patients with IBD. Total RNA was extracted from freshly obtained inflamed and unaffected mucosal biopsies from 15 patients with CD and 18 patients with UC, and analyzed for MIR31 expression by qRT-PCR. Statistical analysis was performed using paired *t*-test. \*\*\**P* < .001. (C) Pearson's correlation analysis was performed between the relative levels of MIR31 expression of intestinal mucosa and CRP (C-reactive protein), ESR (erythrocyte sedimentation rate), Mayo score, and ulcerative colitis endoscopic index of severity (UCEIS) from 52 patients with UC (Spearman's rank correlation coefficient, *R* = 0.5513, *P* < .0001 for CRP; *R* = 0.5060, *P* < .0001 for ESR; *R* = 0.4824, *P* < .0001 for Mayo score; *R* = 0.5982, *P* < .0001 for UCEIS). (D) Pearson's correlation analysis was performed between the relative levels of MIR31 expression of intestinal mucosa and CRP, ESR, CDAI (Crohn's disease activity index), and SES-CD (simple endoscopic score for CD values) from 69 patients with CD (Spearman's rank correlation coefficient, *R* = 0.6514, *P* < .0001 for CRP; *R* = 0.6620, *P* < .0001 for ESR; *R* = 0.6507, *P* < .0001 for CDAI; *R* = 0.5614, *P* < .0001 for SES-CD). (E) qRT-PCR for MIR31 in colonic epithelium at indicated time points after DSS treatment. n = 4 at each time point. Statistical analysis was performed using paired *t*-test. \*\**P* < .01; \*\*\**P* < .001. (F) In situ hybridization for *MIR31* in colons with or without a 5-day DSS treatment. *MIR31*<sup>-/-</sup> colon was used as a negative control. Scale bar: 50  $\mu$ m. The dashed boxes indicate the high magnification images in the bottom panel.



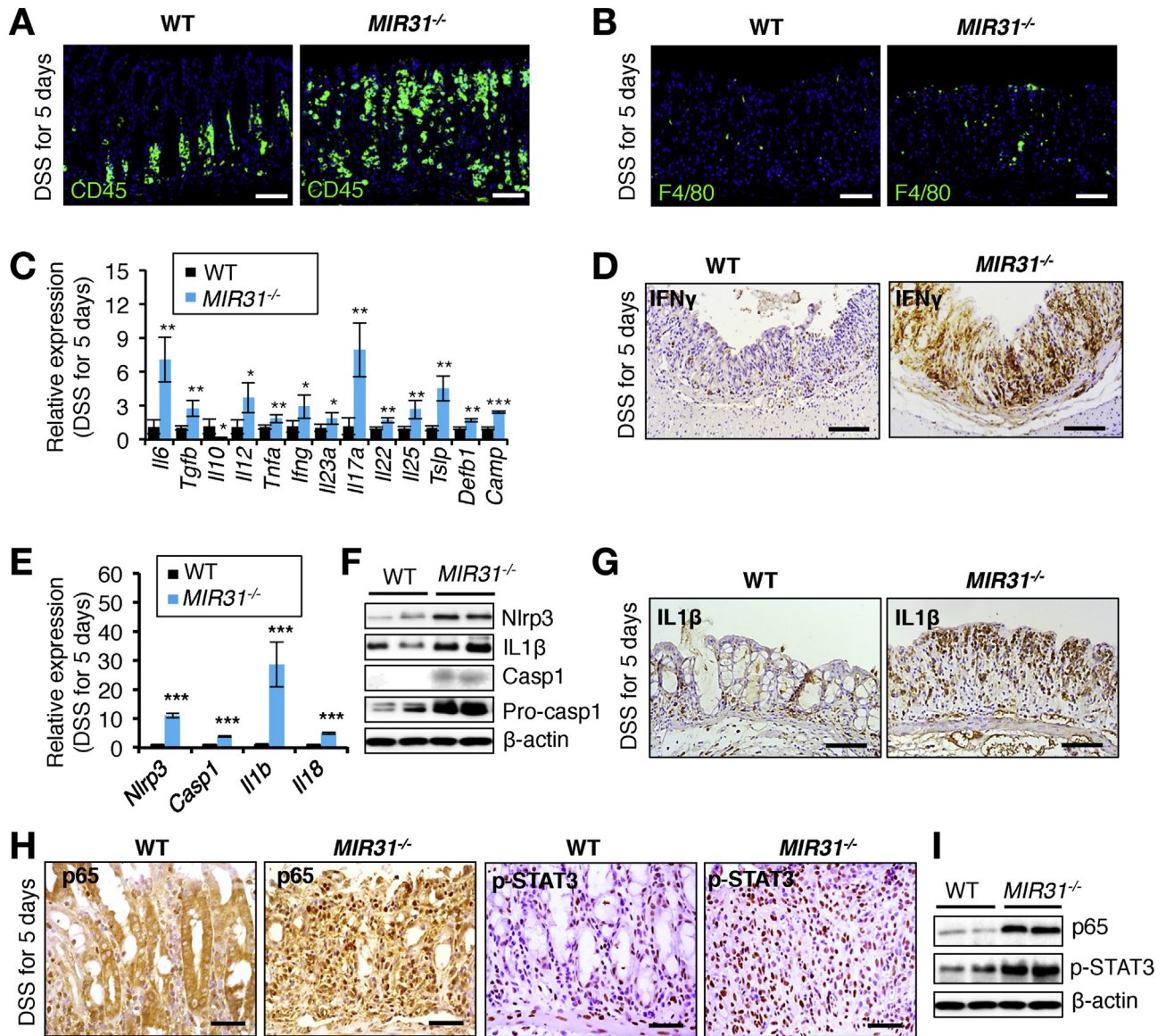
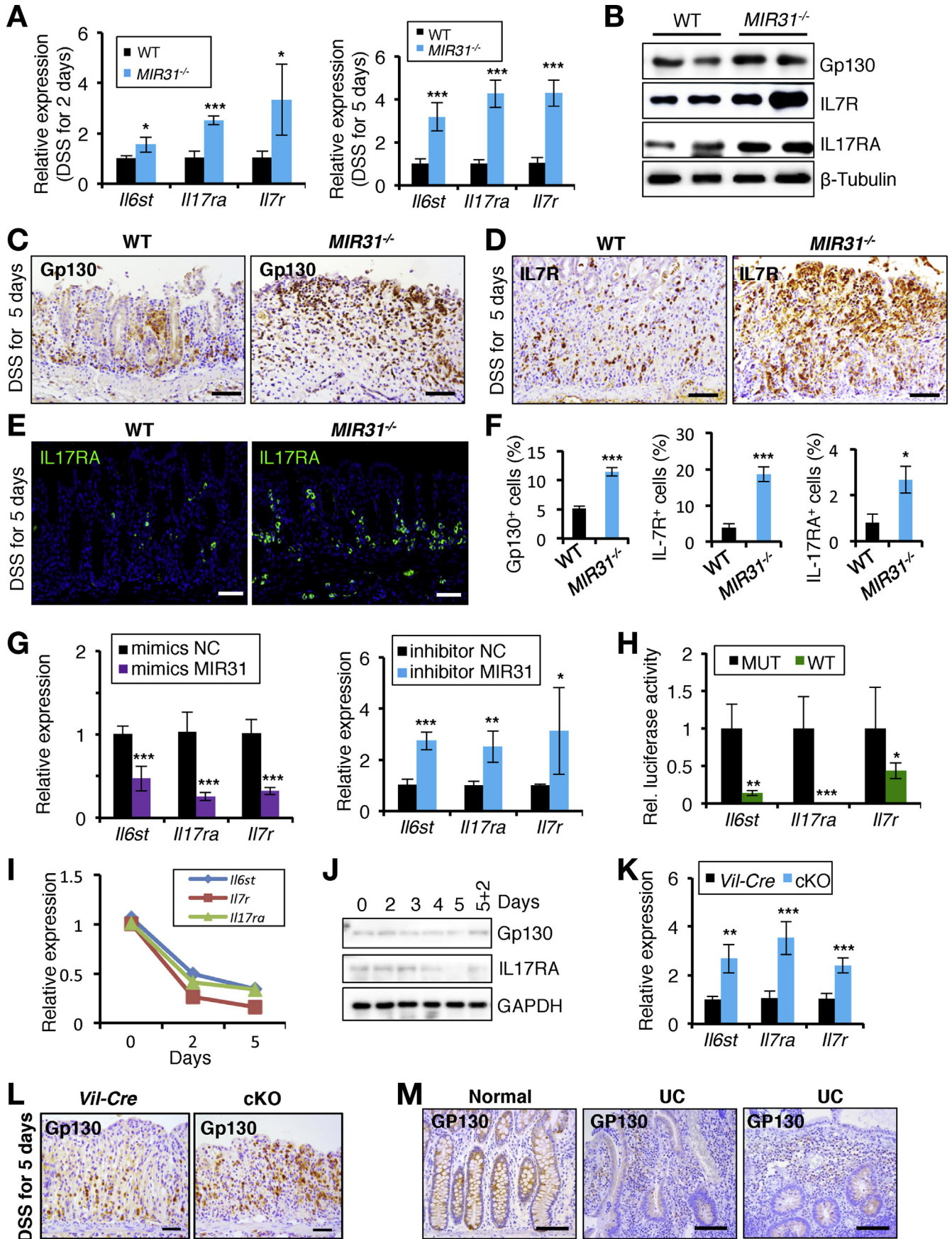


**Figure 3.** Mucosal immunity is hyperreactive in *MIR31*<sup>-/-</sup> mice following DSS treatment. (A and B) Immunofluorescence for CD45 (A) and F4/80 (B) in the colon from control and *MIR31*<sup>-/-</sup> mice following 5 days of DSS treatment. n = 4. Scale bar: 50 μm. (C) Quantitative reverse-transcriptase polymerase chain reaction (qRT-PCR) analysis for *Il6*, *Tgfb*, *Il10*, *Il12*, *Tnfa*, *Ifng*, *Il23a*, *Il17a*, *Il22*, *Il25*, *Tslp*, *Defb1*, and *Camp* in the colon from WT and *MIR31*<sup>-/-</sup> mice following 5 days of DSS treatment. \**P* < .05; \*\**P* < .01. n = 5 biological replicates. (D) Immunohistochemistry for interferon (IFN) $\gamma$  in the colon from WT and *MIR31*<sup>-/-</sup> mice following 5 days of DSS treatment. n = 3. Scale bar: 50 μm. (E) qRT-PCR analysis for *Nlrp3*, *Caspase 1*, *Il1b*, and *Il18* in WT and *MIR31*<sup>-/-</sup> colon following 5 days of DSS treatment. \*\*\**P* < .001. n = 5. (F) Western blotting for *Nlrp3*, *Caspase 1*, and *IL1 $\beta$*  in the colon WT and *MIR31*<sup>-/-</sup> mice after 5 days of DSS treatment.  $\beta$ -actin was used as a loading control. n = 3. (G) Immunohistochemistry for *IL1 $\beta$*  in the colon from WT and *MIR31*<sup>-/-</sup> mice following 5 days of DSS treatment. n = 3. Scale bar: 50 μm. (H and I) Immunohistochemistry (H) and western blotting (I) for p65 and p-STAT3 in the colon from WT and *MIR31*<sup>-/-</sup> mice following 5 days of DSS treatment. Scale bar: 50 μm.  $\beta$ -actin was used as a loading control, which is identical to (F). n = 3. Statistical analysis was performed using independent *t*-test for (C) and (E).

**Figure 2.** Exacerbated immune response and impaired epithelial regeneration in *MIR31*<sup>-/-</sup> mice following DSS treatment. (A) Quantification of weight loss in WT and *MIR31*<sup>-/-</sup> littermates after DSS treatment. n = 11 biological replicates for each genotype. \**P* < .05; \*\**P* < .01. (B) Survival curve of WT and *MIR31*<sup>-/-</sup> mice after DSS treatment. n = 25 biological replicates for both WT and *MIR31*<sup>-/-</sup> mice. \*\*\**P* < .001. (C) Representative gross images of colon and spleen from WT and *MIR31*<sup>-/-</sup> littermates following 5 days of DSS treatment. WT, n = 9; *MIR31*<sup>-/-</sup> mice, n = 9. (D) Quantification of colon length and spleen weight in (C). \*\**P* < .01. (E) Quantification of the clinical scores in WT and *MIR31*<sup>-/-</sup> mice after DSS treatment. WT, n = 7; *MIR31*<sup>-/-</sup>, n = 7. \**P* < .05; \*\*\**P* < .001. (F) Histological images of colonic tissue from WT and *MIR31*<sup>-/-</sup> mice at the indicated time points after DSS treatment. WT, n  $\geq$  6 at each timepoint; *MIR31*<sup>-/-</sup>, n  $\geq$  6 at each timepoint. Scale bar: 50 μm. (G) Double immunofluorescence for Ki67 and  $\beta$ -catenin in colon from WT and *MIR31*<sup>-/-</sup> littermates at indicated time points following DSS treatment. WT, n  $\geq$  6 at each time point; *MIR31*<sup>-/-</sup> mice, n  $\geq$  6 at each time point. Scale bar: 50 μm. Statistical analysis was performed using independent *t*-test for A, B, D, E.





transcripts encoding proteins involved in the intestinal immune response using TargetScan algorithms. Genes containing MIR31 binding sites include *Il6st* (encoding GP130), *Il7r*, and *Il17ra* (Supplementary Figure 9A). The RNA and protein levels of *Il6st*, *Il7r*, and *Il17ra* were significantly increased in the colon of *MIR31*<sup>-/-</sup> mice after DSS treatment (Figure 4A and B). The numbers of GP130<sup>+</sup>, IL7R<sup>+</sup>, and IL17RA<sup>+</sup> cells were significantly increased in *MIR31*<sup>-/-</sup> colon following 5 days of DSS treatment (Figure 4C–F). In addition, in vitro analysis revealed that MIR31 mimics inhibited the expression of *Il6st*, *Il7r*, and *Il17ra*, whereas MIR31 inhibitors promoted their up-regulation (Figure 4G), suggesting that these putative target genes are regulated by MIR31 in a cell autonomous manner. 3'UTR-Luciferase reporter assays revealed that MIR31 mimics significantly suppressed WT *Il6st*, *Il7r*, and *Il17ra* 3'UTR activity but had no significant influence on the reporters in which the MIR31 binding site was mutated (Figure 4H and Supplementary Figure 9B). Expression of *Il6st*, *Il7r*, and *Il17ra* declined over the course of DSS treatment (Figure 4I and J), inversely correlating to the MIR31 level. The up-regulation of these MIR31 target genes was further validated in cKO colon (Figure 4K and L). The reduction in GP130 was also found in human UC tissue (Figure 4M). Together, our findings demonstrate that transcripts of *Il6st*, *Il7r*, and *Il17ra* are direct targets of MIR31, and that their regulation may account for the effect of MIR31 in repression of the immune reaction in intestinal mucosa.

### MIR31 Promotes Epithelial Regeneration by Directly Regulating WNT and Hippo Signaling

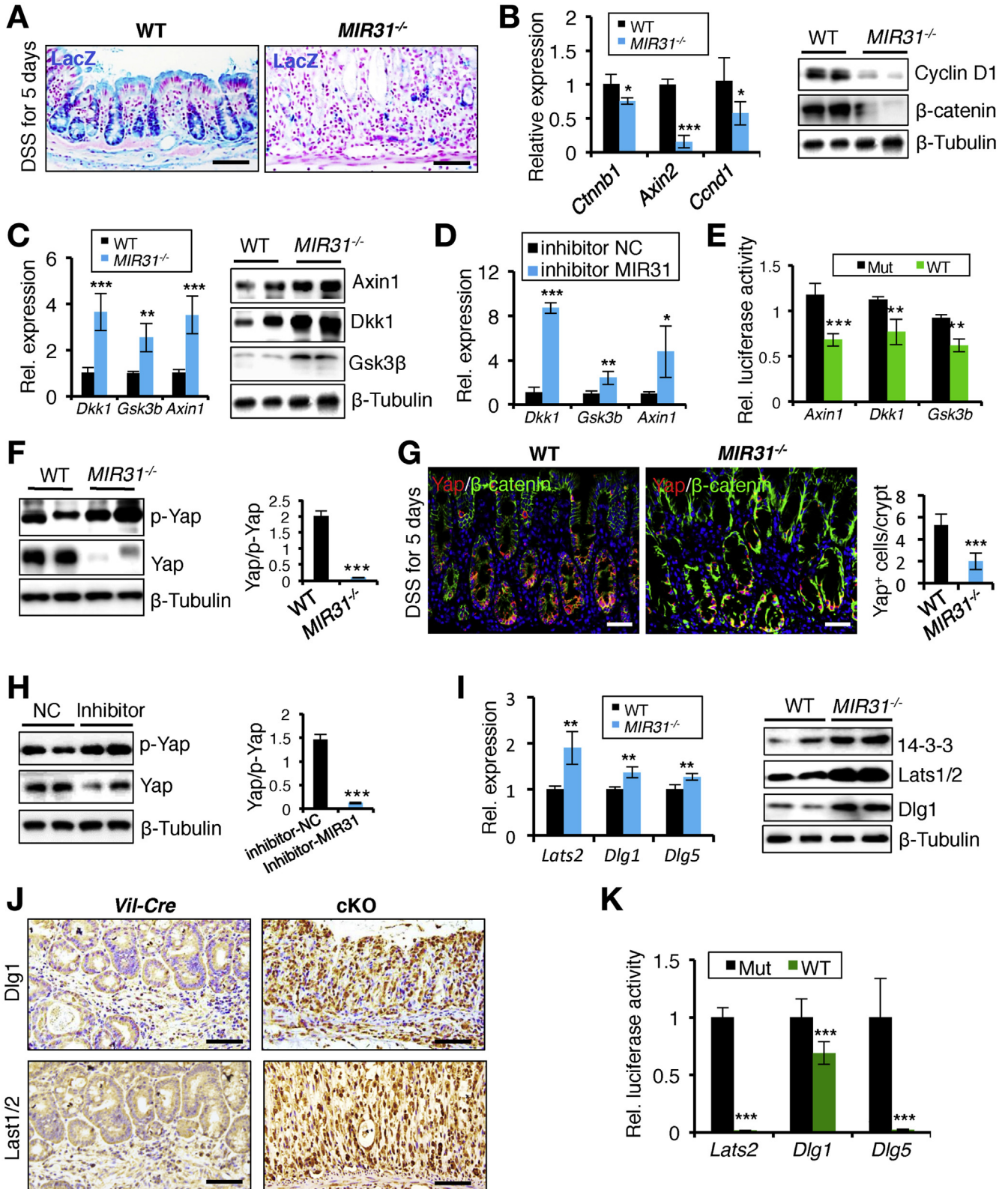
To investigate the molecular mechanisms of MIR31 regulation of immune reaction and epithelial regeneration, we compared colonic epithelial cells transcriptomes between WT (n = 3) and *MIR31*<sup>-/-</sup> (n = 3) mice. We defined the differentially expressed genes as those with *P* < .05 and fold change >1.5. This approach yielded 178 down-regulated genes and 285 up-regulated genes in *MIR31*<sup>-/-</sup> mice (Supplementary Figure 10A). The enriched KEGG pathways included complement and coagulation, sphingolipid metabolism, and transforming growth factor- $\beta$  and WNT signaling pathways (Supplementary Figure 10B). Of

them, activity of the canonical WNT pathway is a major driving force for epithelial regeneration after injury.<sup>19</sup> We recently demonstrated that MIR31 promotes the proliferative expansion of small intestinal stem cells by activating WNT signaling.<sup>16</sup> We thus examined the effect of MIR31 on WNT activity in DSS-induced colitis. We used *Axin2-LacZ* reporter mice as a proxy for activity of the canonical WNT pathway and observed that reporter activity was activated throughout the colonic epithelium in WT mice before or after 5-day DSS treatment, whereas its activity was markedly reduced in the *MIR31*<sup>-/-</sup> colon (Figure 5A and Supplementary Figure 11A). Consistently, the expression levels of *Ctnnb1* (encoding  $\beta$ -catenin) and the WNT target genes, *Ccnd1* (encoding *cyclin D1*) and *Axin2*, were significantly reduced in the colon of *MIR31*<sup>-/-</sup> mice both at the RNA and protein levels after DSS treatment (Figure 5B and Supplementary Figure 11B). In addition, the RNA and/or protein expression levels of *Ccnd1* and *Axin2* were significantly down-regulated in LOVO cells on MIR31 inhibition (Supplementary Figure 11C), whereas the expression of these genes was markedly increased in MIR31-overexpressing cells (Supplementary Figure 11D), suggesting a direct effect of MIR31 on WNT activity. Wnt antagonists *Axin1*, *Gsk3 $\beta$* , and *Dkk1* have been identified as MIR31 targets in intestinal stem cells (Supplementary Figure 9A).<sup>16</sup> In agreement, the levels of these Wnt antagonists were up-regulated in the colon of *MIR31*<sup>-/-</sup> mice after 5 days of DSS treatment (Figure 5C and Supplementary Figure 11E). In contrast, a reduction in DKK1 and AXIN1 was observed in human UC samples (Supplementary Figure 11F). In vitro assays also showed that the expression of these putative target genes was up-regulated on treatment with MIR31 inhibitors (Figure 5D), and down-regulated in response to MIR31 mimics (Supplementary Figure 11G). 3'UTR-luciferase reporter assays revealed that MIR31 mimics significantly suppressed WT *Axin1*, *Gsk3b*, and *Dkk1* 3'UTR activity but had no significant influence on the reporters in which the MIR31 binding site was mutated (Figure 5E and Supplementary Figure 9B). Thus, our findings indicate that MIR31 activates WNT signaling pathway by directly suppressing Wnt antagonists *Axin1*, *Gsk3b*, and *Dkk1* in DSS-induced colitis, consequently promoting epithelial regeneration.

**Figure 4.** MIR31 directly targets *Il6st*, *Il7r*, and *Il17ra* to suppress immune response. (A) Quantitative reverse-transcriptase polymerase chain reaction (qRT-PCR) analysis for *Il6st*, *Il7r*, and *Il17ra* in the colon of WT and *MIR31*<sup>-/-</sup> mice after 2 and 5 days of DSS treatment. \**P* < .05; \*\*\**P* < .001. n = 5. (B) Western blotting for Gp130, IL7R, and IL17RA in the colon of WT and *MIR31*<sup>-/-</sup> mice after 5 days of DSS treatment.  $\beta$ -Tubulin was used as a loading control. n = 3. (C–E) Immunostaining for Gp130 (C), IL7R (D), and IL17RA (E) in the colon of WT and *MIR31*<sup>-/-</sup> mice following 5 days of DSS treatment. Scale bar: 50  $\mu$ m. n = 3. (F) Quantification of Gp130<sup>+</sup>, IL7R<sup>+</sup>, and IL17RA<sup>+</sup> cells in (C–E). n = 3. \**P* < .05; \*\*\**P* < .001. (G) qRT-PCR analysis for *Il6st*, *Il7r*, and *Il17ra* in LOVO colorectal cancer cells on treatment of MIR31 mimics (left) and inhibitor (right). n = 3 technical replicates. \**P* < .05; \*\**P* < .01; \*\*\**P* < .001. (H) Ratio of luciferase activity of MIR31 mimics vs scrambled RNA in WT and mutant 3'UTR constructs for *Il6st*, *Il7r*, and *Il17ra* genes based on 3 independent experiments. \**P* < .05; \*\**P* < .01; \*\*\**P* < .001. n = 3 technical replicates. (I) qRT-PCR analysis for *Il6st*, *Il7r*, and *Il17ra* in WT colon on days 0, 2, and 5 after DSS treatment. n = 3 for each time point. (J) Western blotting for Gp130 and IL17RA in WT colon at indicated time points after DSS treatment. Glyceraldehyde-3-phosphate dehydrogenase (GAPDH) was used as a loading control. n = 3. (K) qRT-PCR analysis for *Il6st*, *Il7r*, and *Il17ra* in *Vil-Cre* and cKO colon 5 days after DSS treatment. \*\**P* < .01; \*\*\**P* < .001. n = 4. (L) Immunohistochemistry for Gp130 in the colon of *Vil-Cre* and cKO mice after 5 days of DSS treatment. n = 3. Scale bar: 50  $\mu$ m. (M) Immunohistochemistry for Gp130 in normal human colon (n = 4) and human UC samples (n = 5). Scale bar: 100  $\mu$ m. Statistical analysis was performed using independent *t*-test for A, F, G, H, and K.

The Hippo signaling pathway is essential for tissue regeneration in the colon after DSS-mediated injury.<sup>6</sup> We found that the Yap::pYap ratio was reduced in the colon of *MIR31*<sup>-/-</sup> mice before DSS treatment (Supplementary

Figure 12A), becoming more pronounced after 5 days of DSS treatment (Figure 5F), suggesting an activation of the Hippo signaling pathway in *MIR31*<sup>-/-</sup> mice. Consistently, the number of Yap<sup>+</sup> cells within colonic epithelium was



significantly reduced after DSS treatment (Figure 5G and Supplementary Figure 12B). Furthermore, we found that MIR31 mimics increased the Yap::pYap ratio in LOVO cells (Supplementary Figure 12C), whereas MIR31 inhibition decreased it (Figure 5H), suggesting a direct effect of MIR31 on Hippo activity. *Ctgf*, *Cyr61*, and *Ankrd1* are well-characterized Yap target genes,<sup>20</sup> and their expression was decreased after 5 days of DSS treatment in the *MIR31*<sup>-/-</sup> mice (Supplementary Figure 12D). In vitro, MIR31 inhibitors significantly suppressed these Yap target genes, whereas MIR31 mimics promoted them (Supplementary Figure 12E and F). Taken together, both in vivo and in vitro findings demonstrate that MIR31 represses the Hippo signaling pathway during DSS-induced colitis.

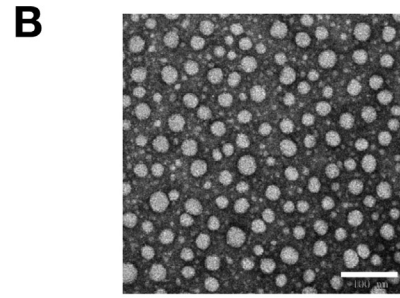
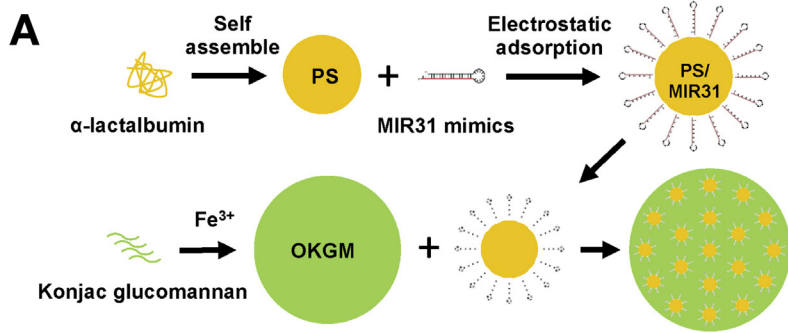
To understand how MIR31 regulates Hippo signaling, we analyzed MIR31 binding sites in the 3'UTRs of transcripts encoding inhibitors of the Hippo pathway using TargetScan algorithms. We found that the 3'UTR in transcripts of *Lats2*, *Dlg1*, and *Dlg5* included MIR31 binding sites (Supplementary Figure 9A), and the RNA and protein levels of *Lats2*, *Dlg1*, and *Dlg5* were up-regulated in the colon of *MIR31*<sup>-/-</sup> mice after DSS treatment (Figure 5I), as well as in LOVO cells treated with MIR31 inhibitors (Supplementary Figure 12G). Conversely, MIR31 mimics suppressed their expression (Supplementary Figure 12G). The numbers of *Dlg1*<sup>+</sup> and *Lats2*<sup>+</sup> cells were increased in MIR31 cKO colonic epithelium following 5 days of DSS treatment (Figure 5J). 3'UTR-luciferase reporter assays revealed that MIR31 mimics significantly repressed WT *Lats2*, *Dlg1*, and *Dlg5* 3'UTR activity, but had no significant influence on the reporters in which the MIR31 binding site was mutated (Figure 5K and Supplementary Figure 9B). These findings indicate that *Lats2*, *Dlg1*, and *Dlg5* transcripts are direct targets of MIR31, accounting for the effect of MIR31 suppressing Hippo signaling pathway. Collectively, our data demonstrate that MIR31 promotes epithelial regeneration

by regulating WNT and Hippo signaling pathways during DSS-induced colitis. Furthermore, the alteration of MIR31-mediated WNT and Hippo signaling pathways was further confirmed in TNBS-induced murine colitis (Supplementary Figure 13A–F).

### MIR31-based OKGM-PS Microsphere Delivery Is Sufficient to Alleviate DSS-induced Inflammation

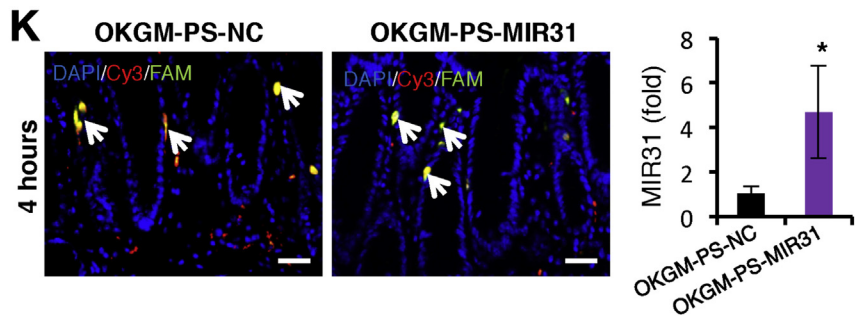
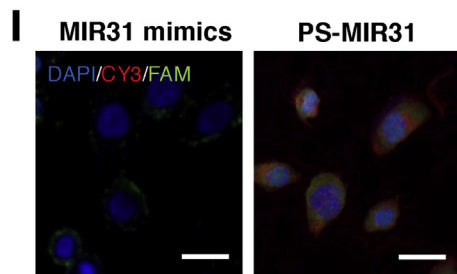
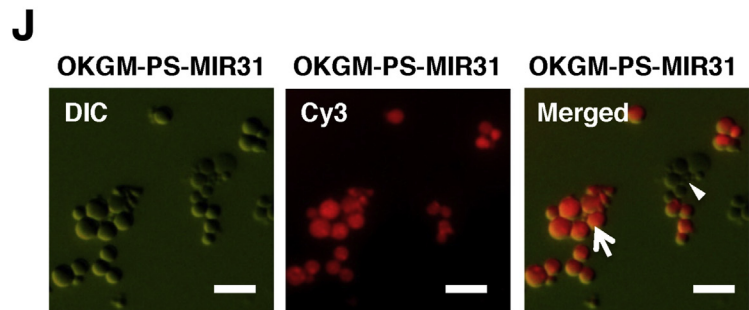
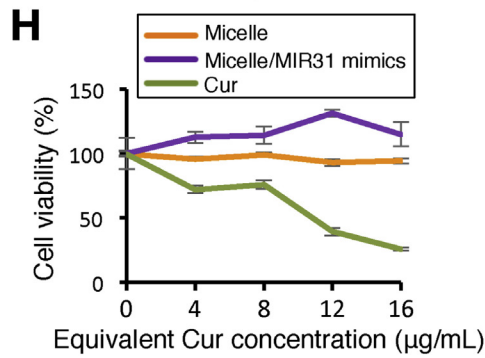
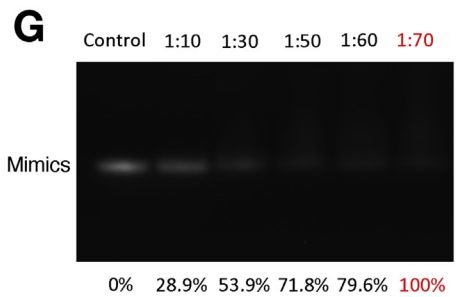
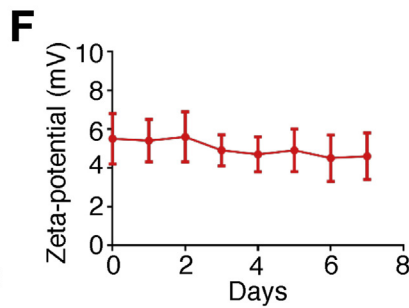
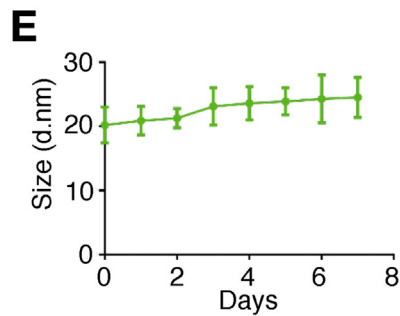
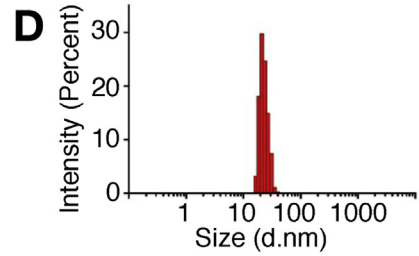
microRNA-based nanodelivery systems have garnered significant interest as therapeutic strategies for a variety of diseases, including IBD.<sup>21</sup> To determine the feasibility of targeting MIR31 with nanoparticles in colitis, we designed a protein-based, encapsulating microsphere as an MIR31 mimic delivery system (Figure 6A). In this system,  $\alpha$ -lactalbumin ( $\alpha$ -La) is partially hydrolyzed at Glu and Asp sites to produce amphiphilic peptides, which can self-assemble into approximately 20-nm peptosomes (PSs)<sup>22</sup> with numerous negatively charged carboxyl groups (Figure 6B and C). To attach MIR31 mimics via electrostatic adsorption, we used maleimide (Mal) to reverse the zeta potential on the surface of PSs (Figure 6C). The size (diameter) and zeta potential of PS+Mal were stable over time (Figure 6D–F). MIR31 mimics were then loaded onto  $\alpha$ -La PSs using Mal (Figure 6G). The MIR31 mimic-loaded PS (PS-MIR31) nanoparticles exhibited low cytotoxicity (Figure 6H) and were capable of delivering MIR31 into cells (Figure 6I). To avoid rapid degradation of the peptide-based nanoparticles in the gut, we encapsulated them inside microspheres formed by cross-linking the carboxyl-abundant TEMPO-oxidized konjac glucomannan (OKGM) with Fe<sup>3+</sup> ions (OKGM-PS-MIR31) (Figure 6J). The size of OKGM-PS-MIR31 microspheres ranged from 10 to 50  $\mu$ m (Figure 6J). The OKGM-PS-MIR31 microspheres were then administered by enema to examine their therapeutic effect in vivo. We found that OKGM-PS-MIR31 can release PS-MIR31 into colonic epithelial cells (Figure 6K), leading to an increase in MIR31

**Figure 5.** MIR31 regulates WNT and Hippo signaling pathways on DSS treatment. (A) WNT activity was evaluated by *Axin2-LacZ* reporter activity in the colon of WT and *MIR31*<sup>-/-</sup> mice following 5 days of DSS treatment. Blue, LacZ signals. n = 3 biological replicates. Scale bar: 50  $\mu$ m. (B) Quantitative reverse-transcriptase polymerase chain reaction (qRT-PCR) analysis for *Ctnnb1*, *Ccnd1*, and *Axin2* (left), as well as western blotting for Cyclin D1 and  $\beta$ -catenin (right) in the colon of WT and *MIR31*<sup>-/-</sup> mice following 5 days of DSS treatment. \**P* < .05; \*\*\**P* < .001.  $\beta$ -Tubulin was used as a loading control. n = 5 biological replicates. (C) qRT-PCR analysis for *Dkk1*, *Gsk3b*, and *Axin1* (left), as well as western blotting for *Dkk1*, *Gsk3 $\beta$* , and *Axin1* (right) in WT and *MIR31*<sup>-/-</sup> colon following 5-day DSS treatment. n = 3 biological replicates. \*\**P* < .01; \*\*\**P* < .001.  $\beta$ -Tubulin was used as a loading control, which is identical to (B). (D) qRT-PCR analysis for *Dkk1*, *Gsk3b*, and *Axin1* in LOVO cells in response to MIR31 inhibitor. \**P* < .05; \*\**P* < .01; \*\*\**P* < .001. n = 3 technical replicates. (E) Ratio of luciferase activity of *MIR31* mimics vs scramble RNA in WT and mutant 3'UTR constructs for *Dkk1*, *Gsk3b*, and *Axin1* genes based on 3 independent experiments. \*\**P* < .01; \*\*\**P* < .001. (F) Western blotting for p-Yap and Yap in the colon from WT and *MIR31*<sup>-/-</sup> littermates following 5 days of DSS treatment. n = 3 biological replicates.  $\beta$ -Tubulin was used as a loading control. Quantification of Yap/p-Yap ratio is shown on the right. \*\*\**P* < .001. (G) Immunofluorescence for Yap in WT and *MIR31*<sup>-/-</sup> colon following 5-day DSS treatment. Scale bar: 50  $\mu$ m. Quantification of Yap<sup>+</sup> cells per crypt is shown on the right. \*\*\**P* < .001. n = 3 biological replicates. (H) Western blotting for p-Yap and Yap in LOVO cells in response to MIR31 inhibitors. n = 3 technical replicates.  $\beta$ -Tubulin was used as a loading control. Quantification of Yap/p-Yap ratio is shown on the right. \*\*\**P* < .001. (I) qRT-PCR analysis for *Lats2*, *Dlg1*, and *Dlg5*, and western blotting for 14-3-3, *Lats1/2* and *Dlg1* in the colon of WT and *MIR31*<sup>-/-</sup> mice following 5 days of DSS treatment. \*\**P* < .01.  $\beta$ -Tubulin was used as a loading control, which is identical to Figure 4B. n = 3 biological replicates. (J) Immunohistochemistry for *Dlg1* and *Lats1/2* in the colon of *Vil-Cre* and cKO mice following 5-day DSS treatment. n = 3 biological replicates. Scale bar: 50  $\mu$ m. (K) Ratio of luciferase activity of *MIR31* mimics vs scramble RNA in WT and mutant 3'UTR constructs for *Lats2*, *Dlg1*, and *Dlg5* genes based on 3 independent experiments. n = 3 technical replicates. \*\*\**P* < .001. Statistical analysis was performed using independent *t*-test for B–I and K.



**C**

	PS	PS - Mal
Zeta-potential	-16.37±1.36 mV	5.57±0.16 mV



levels (Figure 6K), whereas OKGM-PS exhibited no toxicity (Supplementary Figure 14).

We ultimately tested whether the OKGM-PS-MIR31 microspheres could rescue the phenotypes of *MIR31*<sup>-/-</sup> mice in the process of DSS-induced colitis. We fed the *MIR31*<sup>-/-</sup> mice drinking water with 3.5% DSS, and concomitantly administered OKGM-PS-MIR31 microspheres to the large bowel. Compared with treatment with OKGM-PS negative controls, treatment with OKGM-PS-MIR31 microspheres resulted in a slower loss of body weight and abrogated colon shortening (Supplementary Figure 15A-C). The OKGM-PS-MIR31 microsphere-treated *MIR31*<sup>-/-</sup> mice also exhibited reduced inflammation and increased epithelial cell proliferation (Supplementary Figure 15D and E). These findings indicate that the OKGM-PS-MIR31 microspheres can significantly rescue DSS colitis-associated phenotypes in *MIR31*<sup>-/-</sup> mice. We next sought to test the preventive effect of OKGM-PS-MIR31 microspheres against DSS-induced colitis in WT mice. Strikingly, OKGM-PS-MIR31 microspheres alleviated inflammation and the impairment of colonic epithelial integrity, as indicated by an increased body weight, reduced immune response, longer colon length, and increased epithelial cell proliferation (Figure 7A-G). Consistent with our previous findings, WNT and Hippo signaling pathways were altered in the colon of OKGM-PS-MIR31-treated mice (Figure 7G and Supplementary Figure 16A and B), whereas *MIR31* target genes were reduced (Figure 7H and Supplementary Figure 16C). To test its therapeutic efficacy of this system, we first established acute colitis in mice and then treated them with OKGM-PS-MIR31 microspheres. The recovery of body weight and colon length was significantly enhanced in OKGM-PS-MIR31-treated mice (Supplementary Figure 17A-D), concomitant with an organized colonic histology, a reduced inflammatory response, and increased epithelial cell proliferation (Supplementary Figure 17E-G), as well as Hippo signaling

pathway suppression and down-regulation of *MIR31* target gene expression (Supplementary Figure 17H and I). These phenotypes were consistent with the recovery from colitis caused by *MIR31* in vivo overexpression (Supplementary Figure 18A-F), reflecting a high efficiency of OKGM-PS-MIR31 microsphere in delivering *MIR31* mimics. These findings indicated that OKGM-PS-MIR31 microspheres are effective in treating active colitis in mice. Taken together, our findings suggest that OKGM-PS-MIR31 microspheres might be a potent therapeutic approach for treating IBD.

## Discussion

Here, we demonstrated that *MIR31* expression was highly induced in IBD and in experimental murine colitis through activation of NF- $\kappa$ B and STAT3 signaling. In turn, inflammatory signal-induced *MIR31* expression suppressed the immune response of epithelial cells by inhibiting multiple receptors, including GP130, IL17RA, and IL7R, and concomitantly promoted the regenerative capacity of epithelial cells by regulating WNT and Hippo signaling pathways (Supplementary Figure 19).

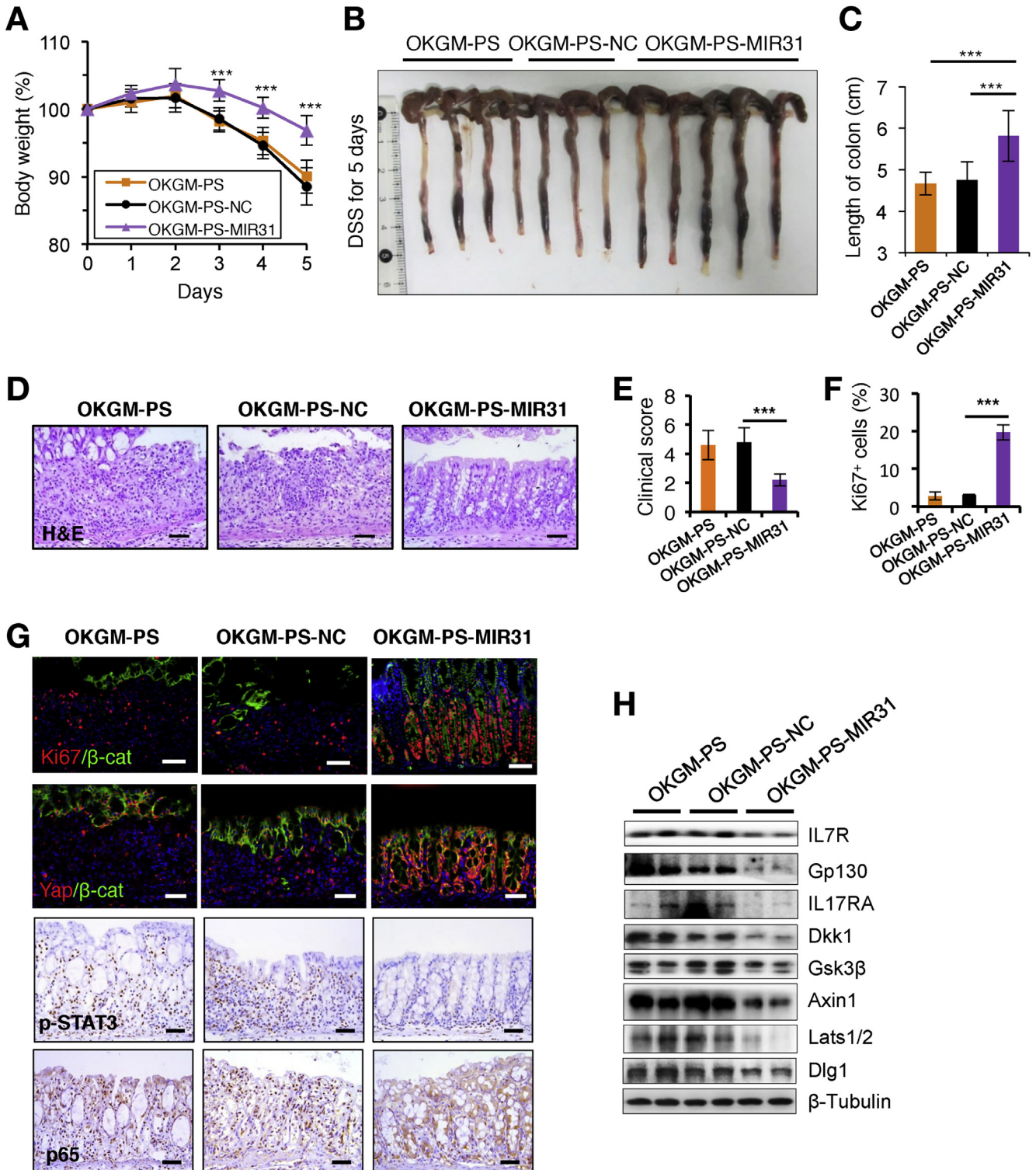
Epithelial cells are known to enhance mucosal immunity by producing proinflammatory cytokines in the inflammatory reaction.<sup>2</sup> Multiple receptors, such as GP130, IL17RA, and IL7R, have been localized to the colonic/intestinal epithelium<sup>3,23,24</sup> and found to respond to signals from immune cells. Among them, IL7/IL7RA and IL6/GP130 can activate STAT3 signaling,<sup>3,25</sup> which is critical for immune function in the epithelium.<sup>26</sup> The interaction between epithelia and immune cells is necessary to rapidly promote mucosal immunity; however, an exacerbated immune response can lead to epithelial barrier dysfunction.<sup>10</sup> Our findings indicate that *MIR31* suppresses the immune response in the epithelium through a negative-feedback loop.

**Figure 6.** Characterization of *MIR31*-based microsphere delivery system consisting of PS-in-OKGM microsphere. (A) Design and synthesis strategy of the OKGM-PS delivery system: PSs were self-assembled by partially hydrolyzed  $\alpha$ -La, then *MIR31* mimics were absorbed to the surface of Mal-modified PSs via electrostatic attraction. PS-MIR31 particles were subsequently encapsulated by OKGM microspheres to form the *MIR31*-based PS-in-OKGM microsphere delivery system (OKGM-PS-MIR31). (B) Transmission electron microscopy images of PSs formed from partially hydrolyzed  $\alpha$ -La. *n* = 5 technical replicates. Scale bar: 100 nm. (C) Zeta potential of hydrolyzed  $\alpha$ -La PS before and after modification with Mal (PS-Mal), in which Mal was linked to the PSs. *n* = 4 technical replicates. (D) Size distribution of PS-Mal micelles by intensity. *n* = 4 technical replicates. (E) Dynamic change in the diameter of PS-Mal micelles over time at room temperature. *n* = 4 technical replicates. (F) Dynamic change in the zeta potential of PS-Mal micelles over time, at room temperature. *n* = 4 technical replicates. (G) Efficiency of *MIR31* mimics loading to PS-Mal micelles. The ratio represents *MIR31* mimic::PS by weight. Bands: *MIR31* mimics. The percentage at the bottom represents the amount of *MIR31* mimic adsorbed to the surface of PS-Mal micelles relative to the original amount of *MIR31* mimics (Control). *n* = 3 technical replicates. (H) CCK-8 analysis of the viability of LOVO cells treated with PS micelle (Micelle), PS-MIR31 micelle (Micelle/*MIR31* mimics), and Curcumin (Cur) at indicated concentrations after 24 hours of incubation. Cur was used as a positive control for cytotoxicity. *n* = 3 technical replicates. (I) Confocal microscopy images showing the internalization of the *MIR31* mimics (labeled by FAM) by LOVO cells delivered without (left) or with (right) PSs (labeled by Cy3) 6 hours after treatment. *n* = 4 technical replicates. Scale bar: 10  $\mu$ M. (J) Microscopy images of OKGM microspheres encapsulating PSs (labeled by Cy3). Left, differential interference contrast image; middle, Cy3 fluorescence image; right, merged image. Arrow points to OKGM-PS microsphere; arrowhead points to OKGM microsphere without PSs. *n* = 4 technical replicates. Scale bar: 20  $\mu$ m. (K) Fluorescence microscopy images showing the intake of PSs (Cy3) and *MIR31* mimics (FAM) or negative control (NC) for *MIR31* mimics (FAM) by epithelial cells in the colon. The mice were treated with *MIR31*-loaded PSs in OKGM microspheres (OKGM-PS-MIR31) or scramble RNA-loaded PSs in OKGM microspheres (OKGM-PS-NC) by enema for 4 hours. *n* = 4 technical replicates. Scale bar: 25  $\mu$ m. Quantitative reverse-transcriptase polymerase chain reaction analysis for *MIR31* in the colon of mice treated with OKGM-PS-NC and OKGM-PS-MIR31 microspheres. \**P* < .05. Statistical analysis was performed using independent *t*-test for (K).

Conversely, MIR31 also promotes epithelial regeneration through the WNT and Hippo signaling pathways.<sup>5-7</sup> Consistent with our findings, previous studies have demonstrated that knockdown of the Wnt antagonist *Dkk1* (a target of MIR31) promotes recovery from intestinal inflammation during acute colitis.<sup>7</sup> Taken together, our

findings identified MIR31 as a critical regulator in suppressing immune response and promoting epithelial regeneration in the inflamed epithelium characteristic of IBD.

Given our findings, MIR31 is an attractive candidate for therapeutic strategies for IBD. We therefore developed an



MIR31-based nanosystem capable of alleviating DSS-induced colitis in mice. To the best of our knowledge, this represents the first microRNA-based nanosystem for IBD treatment. RNA interference-based nanosystems for treating IBD are increasingly emerging. Among them, TNF is often selected as an RNA interference target.<sup>27–29</sup> Although TNF plays an important role in promoting the immune response, the knockdown of TNF is not sufficient to suppress the inflammatory reaction due to the redundant effects of other proinflammatory cytokines. In comparison, the MIR31-based nanosystem can concomitantly target at least 9 genes, including *Il6st* (encoding GP130), *Il7r*, *Il17ra*, *Axin1*, *Gsk3b*, *Dkk1*, *Lats2*, *Dlg1*, and *Dlg5*, making it a more powerful strategy for alleviating inflammation in IBD. To deliver MIR31 efficaciously, we developed a system consisting of OKGM microsphere containing  $\alpha$ -La PSs to release MIR31 mimics, which was characterized by safe, effective, degradable and capable of slow release. The  $\alpha$ -La peptide has been previously described as a safe drug carrier for breast cancer treatment.<sup>22</sup> In our study, MIR31 mimic-loaded PS nanoparticles were protected by larger OKGM microspheres to avoid rapid degradation of PSs and MIR31. The OKGM-PS-MIR31 microspheres were found more stable than liposome- and polysaccharide-based nanoparticles, which are easily degraded by enzymes in the gut.<sup>30,31</sup> Compared with synthetic polymer-based nanocarriers,<sup>32</sup> OKGM-PS-MIR31 microspheres have no stimulatory effects on the immune system and exhibit low toxicity. Therefore, OKGM-PS-MIR31 microspheres represent a safe and effective system with high potential for treating IBD.

## Supplementary Material

Note: To access the supplementary material accompanying this article, visit the online version of *Gastroenterology* at [www.gastrojournal.org](http://www.gastrojournal.org), and at <https://doi.org/10.1053/j.gastro.2019.02.023>.

## References

1. Kim DH, Cheon JH. Pathogenesis of inflammatory bowel disease and recent advances in biologic therapies. *Immune Netw* 2017;17:25–40.
2. Neurath MF. Cytokines in inflammatory bowel disease. *Nat Rev Immunol* 2014;14:329–342.

3. Ernst M, Thiem S, Nguyen PM, et al. Epithelial gp130/Stat3 functions: an intestinal signaling node in health and disease. *Semin Immunol* 2014;26:29–37.
4. Kumar P, Monin L, Castillo P, et al. Intestinal interleukin-17 receptor signaling mediates reciprocal control of the gut microbiota and autoimmune inflammation. *Immunity* 2016;44:659–671.
5. Kuhnert F, Davis CR, Wang HT, et al. Essential requirement for Wnt signaling in proliferation of adult small intestine and colon revealed by adenoviral expression of Dickkopf-1. *Proc Natl Acad Sci U S A* 2004;101:266–271.
6. Deng F, Peng L, Li Z, et al. YAP triggers the Wnt/beta-catenin signalling pathway and promotes enterocyte self-renewal, regeneration and tumorigenesis after DSS-induced injury. *Cell Death Dis* 2018;9:153.
7. Koch S, Nava P, Addis C, et al. The Wnt antagonist Dkk1 regulates intestinal epithelial homeostasis and wound repair. *Gastroenterology* 2011;141:259–268; e1–8.
8. Kuhn KA, Manieri NA, Liu TC, et al. IL-6 stimulates intestinal epithelial proliferation and repair after injury. *PLoS One* 2014;9:e114195.
9. Okamoto R, Watanabe M. Role of epithelial cells in the pathogenesis and treatment of inflammatory bowel disease. *J Gastroenterol* 2016;51:11–21.
10. Martini E, Krug SM, Siegmund B, et al. Mend your fences: the epithelial barrier and its relationship with mucosal immunity in inflammatory bowel disease. *Cell Mol Gastroenterol Hepatol* 2017;4:33–46.
11. Wu F, Zikusoka M, Trindade A, et al. MicroRNAs are differentially expressed in ulcerative colitis and alter expression of macrophage inflammatory peptide-2 alpha. *Gastroenterology* 2008;135:1624–1635.e24.
12. Tili E, Michaille JJ, Piurowski V, et al. MicroRNAs in intestinal barrier function, inflammatory bowel disease and related cancers—their effects and therapeutic potentials. *Curr Opin Pharmacol* 2017;37:142–150.
13. Schaefer JS, Attumi T, Opekun AR, et al. MicroRNA signatures differentiate Crohn's disease from ulcerative colitis. *BMC Immunol* 2015;16:5.
14. Beres NJ, Kiss Z, Sztupinszki Z, et al. Altered mucosal expression of microRNAs in pediatric patients with inflammatory bowel disease. *Dig Liver Dis* 2017;49:378–387.
15. Oлару AV, Selaru FM, Mori Y, et al. Dynamic changes in the expression of MicroRNA-31 during inflammatory bowel disease-associated neoplastic transformation. *Inflamm Bowel Dis* 2011;17:221–231.

**Figure 7.** OKGM-PS-MIR31 microsphere sufficiently alleviate DSS-induced colitis. (A) Quantification of weight loss in WT mice following 5 days of DSS treatment, coupled with OKGM, OKGM-PS-NC, and OKGM-PS-MIR31 treatment.  $n = 6$  biological replicates for each treatment.  $**P < .01$ ;  $***P < .001$ . (B) Representative gross images of the colon of mice treated with OKGM-PS, OKGM-PS-NC, and OKGM-PS-MIR31 following 5 days of DSS treatment.  $n = 6$  biological replicates for each treatment. (C) Quantification of colon length under the different conditions in (B).  $**P < .01$ . (D) Hematoxylin-eosin (H&E) staining in the colon from WT mice following 5 days of DSS treatment, and treated with OKGM-PS, OKGM-PS-NC, and OKGM-PS-MIR31 microsphere. Scale bar:  $50 \mu\text{m}$ . (E) Quantification of the clinical scores in WT mice following 5 days of DSS treatment, coupled with OKGM-PS, OKGM-PS-NC, and OKGM-PS-MIR31 treatment.  $n = 6$  for each treatment.  $***P < .001$ . (F) Quantification of Ki67<sup>+</sup> cells in (G).  $n = 6$  for each treatment.  $***P < .001$ . (G) Double immunofluorescence for Ki67 and  $\beta$ -catenin, Yap and  $\beta$ -catenin, and immunohistochemistry for p-STAT3 and p65 in the colon from WT mice following 5 days of DSS treatment, and treatment with OKGM-PS, OKGM-PS-NC, and OKGM-PS-MIR31 microspheres. Scale bar:  $50 \mu\text{m}$ . (H) Western blotting for MIR31 targets IL7R, Gp130, IL17RA, Dkk1, Gsk3 $\beta$ , Axin1, Lats1/2, and Dlg1 in the colon of WT mice following 5 days of DSS treatment, and treatment with OKGM-PS, OKGM-PS-NC, and OKGM-PS-MIR31 microsphere.  $\beta$ -Tubulin was used as a loading control. Statistical analysis was performed using independent  $t$ -test for A, C, E, and F.

16. **Tian Y, Ma X, Lv C**, et al. Stress responsive miR-31 is a major modulator of mouse intestinal stem cells during regeneration and tumorigenesis. *Elife* 2017;6:e29538.
17. Shi T, Xie Y, Fu Y, et al. The signaling axis of microRNA-31/interleukin-25 regulates Th1/Th17-mediated inflammation response in colitis. *Mucosal Immunol* 2017;10:983–995.
18. **Lv C, Li F, Li X**, et al. MiR-31 promotes mammary stem cell expansion and breast tumorigenesis by suppressing Wnt signaling antagonists. *Nat Commun* 2017;8:1036.
19. Clevers H, Loh KM, Nusse R. Stem cell signaling. An integral program for tissue renewal and regeneration: Wnt signaling and stem cell control. *Science* 2014;346:1248012.
20. Yu FX, Zhao B, Panupinthu N, et al. Regulation of the Hippo-YAP pathway by G-protein-coupled receptor signaling. *Cell* 2012;150:780–791.
21. Chen WX, Ren LH, Shi RH. Implication of miRNAs for inflammatory bowel disease treatment: systematic review. *World J Gastrointest Pathophysiol* 2014;5:63–70.
22. Li Y, Li W, Bao W, et al. Bioinspired peptosomes with programmed stimuli-responses for sequential drug release and high-performance anticancer therapy. *Nanoscale* 2017;9:9317–9324.
23. Zhang Z, Zheng M, Bindas J, et al. Critical role of IL-17 receptor signaling in acute TNBS-induced colitis. *Inflamm Bowel Dis* 2006;12:382–388.
24. Shalpour S, Deiser K, Kuhl AA, et al. Interleukin-7 links T lymphocyte and intestinal epithelial cell homeostasis. *PLoS One* 2012;7:e31939.
25. Palmer MJ, Mahajan VS, Trajman LC, et al. Interleukin-7 receptor signaling network: an integrated systems perspective. *Cell Mol Immunol* 2008;5:79–89.
26. Han J, Theiss AL. Stat3: friend or foe in colitis and colitis-associated cancer? *Inflamm Bowel Dis* 2014;20:2405–2411.
27. Zhang Y, Cristofaro P, Silbermann R, et al. Engineering mucosal RNA interference in vivo. *Mol Ther* 2006;14:336–342.
28. Laroui H, Theiss AL, Yan Y, et al. Functional TNFalpha gene silencing mediated by polyethyleneimine/TNFalpha siRNA nanocomplexes in inflamed colon. *Biomaterials* 2011;32:1218–1228.
29. Kriegel C, Amiji MM. Dual TNF-alpha/Cyclin D1 gene silencing with an oral polymeric microparticle system as a novel strategy for the treatment of inflammatory bowel disease. *Clin Transl Gastroenterol* 2011;2:e2.
30. Xue HY, Guo P, Wen WC, et al. Lipid-based nanocarriers for RNA delivery. *Curr Pharm Des* 2015;21:3140–3147.
31. Chourasia MK, Jain SK. Polysaccharides for colon targeted drug delivery. *Drug Deliv* 2004;11:129–148.
32. Frede A, Neuhaus B, Klopffleisch R, et al. Colonic gene silencing using siRNA-loaded calcium phosphate/PLGA nanoparticles ameliorates intestinal inflammation in vivo. *J Control Release* 2016;222:86–96.

---

Author names in bold designate shared co-first authorship.

Received June 26, 2018. Accepted February 13, 2019.

#### Reprint requests

Address requests for reprints to: Zhengquan Yu, PhD (lead contact), State Key Laboratories for Agrobiotechnology and Beijing Advanced Innovation Center for Food Nutrition and Human Health, and College of Biological Sciences, China Agricultural University, Yuanmingyuan West Rd. 2, Haidian District, Beijing, 100193, China. e-mail: [zyu@cau.edu.cn](mailto:zyu@cau.edu.cn); fax: 86-10-62733904; or Zhanju Liu, MD, PhD, Department of Gastroenterology, The Shanghai Tenth People's Hospital, Tongji University, Shanghai 200072, China. e-mail: [liuzhanju88@126.com](mailto:liuzhanju88@126.com); fax: +86-21-66303983.

#### Acknowledgments

The authors thank the members from the laboratory animal center in China Agricultural University for their assistance of animal care.

Author contributions: Zhengquan Yu and Yuan Li designed the project; Yuhua Tian, Jiuzhi Xu, Yuan Li, Ran Zhao, Xueyun Bi, Sujuan Du, Cong Lv, Xiaole Sheng, Ruiqi Liu, Wei Wu, Zhanju Liu, Mengzhen Li, Xi Wu, Huiwen You, Guilin Li, Pengbo Lou, Bing Zhang, and Yongli Song performed research; Wei Cui, Jinyue Sun, Jianwei Shuai, Fazheng Ren, Kaichun Wu, Lixiang Xue, Hongquan Zhang, Maksim V. Plikus, Yingzi Cong, Xiaohua Hou, Mingzhou Guo, Huiwen You, Zhanju Liu, Zhengquan Yu analyzed data; Yuhua Tian, Christopher J. Lengner, Zhengquan Yu wrote manuscript.

#### Conflicts of interest

The authors disclose no conflicts.

#### Funding

This work was funded by grants from the National Natural Science Foundation of China (81772984, 81572614, 81630017, 91740117); Beijing Nature Foundation Grant (5162018); the Major Project for Cultivation Technology (2016ZX08008001, 2014ZX08008001); Basic Research Program (2015QC0104, 2015TC041, 2016SY001, 2016QC086); and SKLB Open Grant (2018SKLAB6-12).



## Supplementary Materials and Methods

### Ethics

All mouse experimental procedures and protocols were evaluated and authorized by the Beijing Laboratory Animal Management and were performed strictly in accordance with the guidelines of the Institutional Animal Care and Use Committee of China Agricultural University (approval number: SKLAB-2011-04-03).

### In Situ Hybridization

The MIR31 in situ hybridization assay was performed as described previously with modifications.<sup>1</sup> Digoxigenin-labeled LNA probes (Exiqon, Vedbaek, Denmark) were used following the manufacturer's protocol. Both digoxigenin-labeled MIR31 and scrambled LNA probes (Exiqon) were hybridized at 61°C. The U6 probe was used as a positive control. In situ signals were detected by staining with anti-digoxigenin-AP antibody (Roche, Basel, Switzerland) and developed using BM purple substrate (Roche).

### DSS Treatment

Mice were treated with 3.5% wt/vol DSS with molecular weight 36,000 to 50,000 (MP Biochemicals, Santa Ana, CA) in drinking water for 5 days and DSS was withdrawn for another 3 days. The severity of colitis was scored daily by recording standard parameters, including body weight as well as the presence of diarrhea, and bloody stools. The colonic tissues were removed and fixed in 10% paraformaldehyde for 24 hours, embedded in paraffin, sectioned, and stained with hematoxylin and eosin. The histological grade of colonic inflammation was graded from 0 to 4 as previously described.<sup>2</sup> The disease activity index was measured as previously reported.<sup>2</sup> Clinical scores were evaluated by an independent investigator who was blinded to the experiment.

### TNBS Treatment

TNBS induced-colitis was generated as described previously.<sup>3</sup> To induce acute TNBS colitis, the mice were weighed and anesthetized with isoflurane-mixed gas and 150  $\mu$ L of 1% (wt/vol) TNBS (catalog no. p2297; Sigma, Darmstadt, Germany) presensitization solution was applied to a 1.5  $\times$  1.5-cm shaved area of skin on the back of the mouse between the shoulders. On day 8, after weighing and anesthetizing the mice, we slowly injected 125  $\mu$ L of 2.5% (wt/vol) TNBS solution into the lumen of the colon with a 1-mL syringe and 3.5-F catheter and removed the catheter and positioned the mouse head down for 5 minutes. The severity of colitis was scored daily by recording standard parameters including body weight, diarrhea, and bloody stools. The mice were killed at the time points of choice for colon samples.

To induce chronic TNBS colitis, the mice were presensitized as described previously on day 1 and 100  $\mu$ L of designated concentration TNBS was intrarectally administered to the mice at designated time points as previously

described.<sup>3</sup> During this process, animal weight and signs of distress were monitored daily. The mice were killed after 6 cycles of TNBS treatments.

### Quantitative Reverse-Transcriptase Polymerase Chain Reaction Analysis

Quantitative reverse-transcriptase polymerase chain reaction (PCR) analysis was performed to determine the expression levels of MIR31 and coding genes in human and mouse colon tissues. To detect expression of MIR31, reverse transcription was carried out using TaqMan microRNA RT Kit (ABI, Carlsbad, CA). Real-time PCR was carried out in triplicate using the TaqMan Universal Master Mix II. The expression levels of MIR31 were normalized to the levels of U6 snRNA. To detect mRNA level, reverse transcription was carried out using oligo (dT) primers. Real-time PCR was performed using LightCycler 480 SYBR Green I master mix. Glyceraldehyde-3-phosphate dehydrogenase was used as the internal control. The primers used are located in [Supplementary Table 2](#).

### Isolation of Colonic Epithelial and Mesenchymal Cells

IECs were isolated as described previously.<sup>2,4</sup> Briefly, the large intestine was removed and placed in cold Dulbecco's phosphate-buffered saline (DPBS) to remove debris. The colon was opened longitudinally and cut into pieces 1 to 2 cm in size, which were then incubated in 1 $\times$  DPBS containing 5 mM EDTA and 0.2 mM dithiothreitol for 30 minutes at 4°C on a rotating platform to isolate primary IECs. Suspended epithelial cells were collected following gentle vortexing. After isolating the epithelial cells, the remaining tissue was incubated in digestion solution containing 1.5% fetal bovine serum, 1.0 mg/mL collagenase B (Roche Diagnostics GmbH, Mannheim Germany) and 0.1 mg/mL DNase (Sigma) for 1 hour at 37°C. Single mesenchymal cells were collected with centrifuge.

### Intestinal Permeability Assay

WT and *MIR31*<sup>-/-</sup> littermates were fasted for 4 hours, and administered fluorescein isothiocyanate (FITC) dextran tracer (40 kDa, 0.6 mg/g body weight) intragastrically in 0.1 mL of phosphate-buffered saline (PBS); hemolysis-free serum was then collected after 3 hours (using convenient method). A standard curve for a FITC-dextran was ascertained by serially diluting a known amount of FITC-dextran in mouse serum. The samples were diluted using PBS, and the absorbance at 520 nm was measured using a Hitachi (Tokyo, Japan) F-4500 Fluorescence Spectrophotometer.

### Cell Culture and Transfection

LOVO human colorectal cancer cells were cultured under standard culture conditions. TNF (RMTNFAI; ThermoFisher, Waltham, MA) and IL6 (PMC0061; GibcoTM, Waltham, MA) were used to stimulate cells and induce an inflammatory response. Colonic epithelial cells were transfected using Lipofectamine 2000 reagent with 100 nM of

MIR31-5p mirVana microRNA mimics (mimic-MIR31) or the negative control (mimic-NC) or MIR31-5p mirVana microRNA inhibitor (inhibitor-MIR31) or the scramble RNA (inhibitor-NC) according to the manufacturer's protocol (Invitrogen, Carlsbad, CA). The sequence of inhibitor-MIR31 is 5'-AGCUAUGCCAGCAUCUUGCCU-3'. The sequence of inhibitor-NC is 5'-CAGUACUUUUGUGUAGUACAA-3'. The sequence of MIR31 mimics-MIR31:

5'-AGGCAAGAUGCUGGCAUAGCU-3'  
3'-CUAUGCCAGCAUCUUGCCUUU-5'

The sequence of negative control for mimics-NC:

5'-UUCUCCGAACGUGUCACGUUU-3'  
3'-ACGUGACACGUUCGGAGAAUU-5'

### Histology, Immunofluorescence, and Immunohistochemistry

For histological analysis, the colon was rinsed with 1× DPBS, fixed in 10% formalin, paraffin-embedded, and sectioned at 5 μm. The sections were deparaffinized with xylene (2× 15 minutes) followed by treatment with serial dilutions of ethanol (100%, 100%, 95%, 95%, 80%, and 70% for 5 minutes at each step) and 2 washes with double-distilled water (ddH<sub>2</sub>O). The sections were stained with hematoxylin for 10 minutes at room temperature (RT) and then washed in running water for 5 minutes. The sections were stained with eosin for 20 seconds, dehydrated with serial dilutions of ethanol (95%, 95%, 100%, and 100% for 5 minutes at each step), and then mounted with coverslips in neutral gum mounting medium.

For immunofluorescence, antigen retrieval was performed by heating slides in 0.01 M citrate buffer (pH 6.0) in a microwave. Sections were rinsed 3 times with ddH<sub>2</sub>O, immersed in 3% H<sub>2</sub>O<sub>2</sub> for 20 minutes, washed once with TBS-T (TBS, 0.1% Tween-20) and twice with PBS and blocked for 1 hour with blocking solution (10% normal goat serum [5425; Cell Signaling Technology, Danvers, MA] in TBS-T). The sections were incubated with anti-Ki67 (1:150; Leica, Wetzlar, Germany), anti-CD45 (1:200; Santa Cruz, Dallas, TX), anti-F4/80 (1:200; Santa Cruz), anti-IL1β (1:200; Santa Cruz), anti-β-catenin (1:500; Sigma), anti-Gp130 (1:200; Santa Cruz), anti-IL7R (1:200; Santa Cruz), anti-IL-17RA (1:200; Santa Cruz), anti-Cyclin D1 (1:50; Abcam, Cambridge, UK), anti-Axin1 (1:100; Cell Signaling Technology), anti-Gsk3β (1:2000; Abcam), anti-Dkk1 (1:50; Santa Cruz), anti-Yap (1:400; Cell Signaling Technology), anti-Lats1/2 (1:1000; Cell Signaling Technology), anti-Dlg1 (1:1000; Cell Signaling Technology), anti-BrdU (1:50; Abcam), anti-mucin2 (1:100; Santa Cruz), anti-claudin1 (1:200; Cell Signaling), anti-p65 (1:400; Cell Signaling), and anti-p-STAT3 (1:800; Cell Signaling) overnight at 4°C. After incubation with the antibodies, sections were washed 3 times with TBS-T and incubated for 1 hour at RT with Alexa Fluor 488 Goat anti-mouse or anti-rabbit immunoglobulin G (H+L) (Beyotime, Biotechnology, Shanghai, China). The sections were then washed 3 times with TBS-T and stained with 4',6-diamidino-2-phenylindole for 8 minutes, followed by covering sections with agent for quenching resistance.

### Dual Luciferase Activity Assays

To generate reporter constructs for luciferase assays, 300–base pair (bp) to 600 bp fragments containing predicted MIR31 target site in the 3'UTRs of *Il6st*, *Il7r*, *Il17ra*, *Axin1*, *Dkk1*, *Gsk3β*, *Lats2*, *Dlg1*, and *Dlg5* were cloned into the psi-CHECK2 vector (Promega, Madison, WI) between the XhoI and NotI sites, immediately downstream of the *Renilla* luciferase gene. To generate reporters with mutant 3'UTRs, nucleotides in the MIR31 binding site were mutated using a QuikChange Site-Directed Mutagenesis kit (Stratagene, San Diego, CA). For the 3'UTR assays, 293T cells were cotransfected with the vectors, mimics-NC and mimics-MIR31, as well as inhibitor-NC and inhibitor-MIR31, respectively. After 24 hours, latter firefly and renilla luciferase activities were measured using the Dual-Glo luciferase assay according to the manufacturer's instructions (Promega) and then calculated using the following formula: (WT-mimic/WT-mimic-NC)/(MUT-mimic/MUT-mimic-NC). The primers used for amplifying 3'-UTRs of MIR31 target genes are shown in [Supplementary Table 3](#).

### Western Blotting

Tissues or cell lysates were subjected to western blotting according to standard procedures. Frozen tissue biopsies were homogenized using immunoprecipitation (IP) buffer (Beyotime Biotechnology, Shanghai, China), followed by treatment with TissueLyserLT. After the protein concentration was measured using a BCA protein assay kit (Beyotime), 30 μg of total protein was separated by 8% to 12% sodium dodecyl sulfate–polyacrylamide gel electrophoresis under denaturing conditions and transferred to polyvinylidene difluoride membranes (GE Healthcare, Little Chalfont, UK). The polyvinylidene difluoride membranes were blocked with 5% nonfat dry milk and incubated for 1 hour at RT. The following antibodies were applied: phospho-STAT3 (Tyr705), STAT3, anti-glyceraldehyde-3-phosphate dehydrogenase (Sigma), anti-β-Tubulin (Sigma), anti-cyclin D1 (Santa Cruz), anti-β-catenin (Sigma), anti-Dkk1 (Santa Cruz), anti-Gsk3β (Abcam), anti-Axin1 (Cell Signaling), anti-p-p65 (Cell Signaling), anti-Gp130 (Santa Cruz), anti-IL7R (Santa Cruz), anti-IL17RA (Santa Cruz), anti-Lats1/2 (Cell Signaling), anti-Dlg1 (Cell Signaling), anti-IL1β (Cell Signaling), anti-interferon-γ (Santa Cruz), anti-YAP (Cell Signaling), anti-p-YAP (Cell Signaling), anti-14-3-3 (Abcam), anti-CD45 (Santa Cruz), anti-Nlrp3 (Cell Signaling), and anti-caspase1 (Santa Cruz). Protein bands were quantified using Image Lab software (Bio-Rad, Hercules, CA).

### Luciferase Assay for MIR31 Promoter Activity

The sequence of primary MIR31 is located at chromosome 4, NC\_000070.6 (88910557..88910662, complement) in the mouse genome. The 2-kb region upstream of transcript start site was identified as the MIR31 promoter in this study, which is located at chromosome 4, NC\_000070.6 (88910663..88912663) and was cloned into the pGL3-Basic reporter constructs. Binding sites 1 and 2 of p65 are located at 88912038–88912048 and 88912409–88912419,

respectively. The binding site of STAT3 is located at 88911572–88911582. Nucleotides at MIR31 binding site were mutated using QuikChange Site-Directed Mutagenesis kit (Stratagene). The WT and mutant plasmid were transcribed to cells with TK plasmid, respectively. At 24 hours after transfection, firefly and renilla luciferase activities were measured using the Dual-Glo luciferase assay according to the manufacturer's instructions (Promega).

### Chromatin Immunoprecipitation Assay

Using the simple chromatin IP (ChIP) enzymatic chromatin immunoprecipitation kit (#9002; Cell Signaling Technology), ChIP assay was performed according to the manufacturer's protocol with minor modifications. Harvested cells were first cross-linked with 1% (vol/vol) formaldehyde for 10 minutes at RT. After isolating nuclei by the lysis of cytoplasmic fraction, the cells were incubated with micrococcal nuclease (400 gel units) for 20 minutes at 37°C to further digest chromatin into fragments of 150 to 900 bp. The sonicated nuclear fractions were divided for input control and incubated at anti-p65, anti-p-STAT3, H3 as a positive control, and immunoglobulin G as a negative control at 4°C for overnight. The recruited genomic DNA obtained from the ChIP assay was quantified by quantitative PCR with primers specific to p-Stat3 and p65 binding elements of the *MIR31* promoter regions. Primers were as follows: p-STAT3-binding site forward: 5'-TCCAGGCAA-GAAAGTGAGGG -3'; p-STAT3-binding site reverse: 5'-TGAGTAACAGTGCACAGAGC-3'; p65-binding site forward: 5'-AGATACCACCAAGACCCACC -3'; p65-binding site reverse: 5'-GGTGACCAGGGAGATTCGAA-3'.

### Generation of MIR31-Based PSs

A total of 3 mg of  $\alpha$ -La was partially hydrolyzed by 2  $\mu$ L *Bacillus licheniformis* protease in 3 mL of Tris-HCl buffer (75 mM, pH 7.4) at 50°C for 30 minutes. PSs were formed by self-assembly at 4°C overnight. N-(2-Aminoethoxy) malimide (Mal) was conjugated with the -COOH groups on the surface of PSs after EDC activation for 2 hours (the micelle:Mal:EDC weight ratio was 4:1:1). Excess EDC, Mal was removed using a centrifugal filter device (3 kDa, Amicon Ultra-4; Millipore Co., Darmstadt, Germany) at 4000 rpm for 20 minutes. MIR31 mimic was then added into the PSs at Micelle::MIR31 mimics weight ratio of 70:1, and vortexed gently for 10 seconds and stored at 4°C.

### Characterization of PS-MIR31 Nanoparticles

The size distribution and zeta  $\zeta$ -potential of  $\alpha$ -La PSs in ddH<sub>2</sub>O at pH 7.4 were analyzed by dynamic light scattering (Zetasizer Nano ZS90, Worcestershire, UK) at RT. Before the measurement, the samples were diluted properly to reduce multiple scattering effects. The measurements were performed in triplicate.

### Preparation of OKGM-PS-MIR31 Microspheres

OKGM microspheres were prepared by an inverse-emulsion method described in previous work.<sup>5</sup>  $\alpha$ -La PSs

were prepared via self-assembly of partial hydrolyzed protein according to previous work.<sup>6</sup> PS-MIR31 particles were then encapsulated inside the OKGM microspheres via an inverse-emulsion cross-linking method. Subsequently, 25 mg of DO80 (Degree of oxidation of 80%) OKGM polymer, 6 mg of FeSO<sub>4</sub>·7H<sub>2</sub>O and 3 mg of PS-MIR31 were dissolved in 500  $\mu$ L deionized water, and 0.75 g Span80 was dissolved in 20 mL paraffin oil. The water phase was gradually added into the oil phase under mild stirring to form a water-in-oil emulsion. Air was then bubbled through the emulsion at 35 °C under mildly stirring for 4 hours to oxidize Fe<sup>2+</sup> into Fe<sup>3+</sup>, leading to cross-linking of OKGM in the aqueous droplets. Finally, the microparticles were washed 3 times with hexane to remove paraffin oil and another 3 times with methanol to remove hexane. After the washing step, the system was centrifuged (3000g, 2 minutes), the liquid was decanted, and the particles were resuspended. After the last washing step, the OKGM-PS-MIR31 gel particles were stored in 2 mL of pH 3 HCl aqueous solution.

### Application of OKGM-PS-MIR31 Microspheres in Mice

In preventive mode, 150  $\mu$ L of OKGM-PS-MIR31 microsphere (21  $\mu$ g/mL) was administered by enema once per day for 7 consecutive days. Drinking water with 3.5% DSS was provided to the mice for 5 days starting 2 days after the microsphere treatment. Samples were collected immediately after DSS treatment. In the therapeutic model, 3.5% DSS drinking water was administered to the mice for 5 days. Immediately thereafter, the mice were treated with 150  $\mu$ L of OKGM-PS-MIR31 microspheres (21  $\mu$ g/mL) once per day for 7 consecutive days. Samples were collected after microsphere treatment.

### Flow Cytometry of LacZ<sup>+</sup> Cells

*Axin2-LacZ* mice were treated with OKGM-PS, OKGM-PS-NS, and OKGM-PS-MIR31 microspheres 2 times daily for 4 consecutive days. Dissected colons were incubated with 7.5 mM EDTA and 1 mM dithiothreitol in Hank's balanced salt solution for 30 minutes at 37°C, and single-cell suspensions of colonic epithelium were produced following 2.5 U Dispase (BD Biosciences, San Jose, CA) treatment and passing cells through a 40- $\mu$ m cell strainer. The flow cytometry of LacZ<sup>+</sup> cells was performed as described previously with modifications.<sup>7,8</sup> Cells were loaded for 1 minute with hypotonic fluorescein digalactoside (F-1930; Invitrogen) according to the manufacturer's protocol, and then suspended in staining medium (PBS, 4% [vol/vol] fetal calf serum, 10 mM HEPES, pH 7.2) to stop this reaction. Then, the cells were incubated with CD326-PE (EpCAM-PE) (12-5791-81; eBioscience, San Diego, CA). Fixable Viability Dye eFluor 450 (65-0863-14; Invitrogen) was used to exclude dead cells.  $\beta$ -galactosidase hydrolyzes fluorescein digalactoside to fluorescein, with excitation at 491 nm and emission at 514 nm. Flow cytometry analysis was performed on a BD FACS Diva 8.0.1 (BD Pharmingen, Franklin lakes, NJ) and LacZ<sup>+</sup> cells were analyzed using the Flow-Jo (Ashland, OR) 7.6.1 program.

## References

1. **Tian Y, Ma X, Lv C**, et al. Stress responsive miR-31 is a major modulator of mouse intestinal stem cells during regeneration and tumorigenesis. *Elife* 2017;6:e29538.
2. **He C, Shi Y**, Wu R, et al. miR-301a promotes intestinal mucosal inflammation through induction of IL-17A and TNF-alpha in IBD. *Gut* 2016;65:1938–1950.
3. Wirtz S, Popp V, Kindermann M, et al. Chemically induced mouse models of acute and chronic intestinal inflammation. *Nat Protoc* 2017;12:1295–1309.
4. Aaltonen T, Adelman J, Akimoto T, et al. Search for the associated production of the standard-model Higgs Boson in the all-hadronic channel. *Phys Rev Lett* 2009;103:221801.
5. Chen X, Wang S, Lu M, et al. Formation and characterization of light-responsive TEMPO-oxidized konjac glucomannan microspheres. *Biomacromolecules* 2014;15:2166–2171.
6. Li Y, Li W, Bao W, et al. Bioinspired peptosomes with programmed stimuli-responses for sequential drug release and high-performance anticancer therapy. *Nanoscale* 2017;9:9317–9324.
7. **Berg T, Rountree CB, Lee L**, et al. Fibroblast growth factor 10 is critical for liver growth during embryogenesis and controls hepatoblast survival via beta-catenin activation. *Hepatology* 2007;46:1187–1197.
8. Asahina K, Tsai SY, Li P, et al. Mesenchymal origin of hepatic stellate cells, submesothelial cells, and perivascular mesenchymal cells during mouse liver development. *Hepatology* 2009;49:998–1011.

---

Author names in bold designate shared co-first authorship.

**Supplementary Table 1.** Characteristics of Patients with IBD and Healthy Controls (HCs)

	HC	CD	UC
Number of patients	34	79	82
Age (y)	38.2 ± 11.8	35.3 ± 10.2	45.8 ± 13.1
Gender			
Male	16	42	51
Female	18	37	31
Active/Remission		41/38	45/37
Disease duration (mo)		37.3 ± 17.2	34.4 ± 18.1
Current therapy			
5-aminosalicylates		23	61
Salazosulfapyridine		0	4
Azathioprine		62	4
Glucocorticoids		23	57
Methotrexate		13	2
Biologics		48	8
Nutritional therapy		31	5

**Supplementary Table 2.** Primers for Quantitative Reverse-Transcriptase Polymerase Chain Reaction in this Study

Gene	Forward primer 5'–3'	Reverse primer 5'–3'
<i>Axin1</i>	TTCTGGGTTGAGGAAGCAGC	GATTAGGGGCTGGATTGGGT
<i>Dkk1</i>	TCCGAGGAGAAATTGAGGAA	CCTGAGGCACAGTCTGATGA
<i>Gsk3β</i>	CCAACAAGGGAGCAAATTAGAGA	GGTCCCGCAATTCATCGAAA
<i>Ctnnb1</i>	TCCTAGCTCGGGATGTTAC	TTCTGCAGCTTCCTTGTCT
<i>lfn3</i>	ATGAACGCTACACACTGCATC	CCATCCTTTTGCCAGTTCCTC
<i>Tnfa</i>	CCCTCACACTCAGATCATCTTCT	GCTACGACGTGGGCTACAG
<i>Il6</i>	GCCAGAGTCCTTCAGAGAGA	GGTCTTGGTCTTAGCCACT
<i>Tgfb</i>	CTCCCCTGGCTTCTAGTGC	GCCTTAGTTTGGACAGGATCTG
<i>Il10</i>	GCTCTTACTGACTGGCATGAG	CCGAGCTCTAGGAGCATGTG
<i>Il12</i>	TGGTTTGCCATCGTTTTGCTG	ACAGGTGAGGTTCACTGTTTCT
<i>Pink1</i>	TTCTTCGGCCAGTCGGTAG	CTGCTTCTCCTCGATCAGCC
<i>Map1lc3a (Lc3a)</i>	GACCGCTGTAAAGAGGTGC	CTTGACCAACTCGCTCATGTTA
<i>Map1lc3b (Lc3b)</i>	TTATAGAGCGATACAAGGGGGAG	CGCCGTCTGATTATCTTGATGAG
<i>Bnip3</i>	TCCTGGGTAGAAGTGCATTC	GCTGGGCATCCAACAGTATTT
<i>Nlrp3</i>	ATTACCCGCCCCGAGAAAAGG	TCCGAGCAAAGATCCACACAG
<i>Caspase1</i>	ACAAGGCACGGGACCTATG	TCCCAGTCAGTCTGGAATG
<i>IL1b</i>	TACCTGTGTCTTCCCGTGG	TTGTTTCATCTCGGAGCCTGT
<i>Il18</i>	GTCTACCCTCTCCTGTAAAGAACA	TGGCAAGCAAGAAAGTGTCC
<i>Il23a</i>	ATGCTGGATTGCAGAGCAGTA	ACGGGGCACATTATTTTTAGTCT
<i>Il17a</i>	TTTAACTCCCTTGGCGCAAAA	CTTTCCCTCCGCATTGACAC
<i>Il6st</i>	CTCTGTTGACAAGCAATGAGACG	TCTTCAGTATGTCTAGCCCCTG
<i>Il7r</i>	GCGGACGATCACTCCTTCTG	AGCCCCACATATTTGAAATTCCA
<i>Il17ra</i>	AGTGTTCCTCTACCCAGCAC	GAAACCGCCACCGCTTAC
<i>Axin2</i>	GGCTAGCTGAGGTGTCTGAAG	GCCAGTTTCTTTGGCTCTTT
<i>Ccnd1</i>	TGGTGAACAAGCTCAAGTGG	GGCGGATTGGAATGAACT
<i>Ctgf</i>	GGGCCTCTTCTGCGATTTCT	ATCCAGGCAAGTGCATTGGTA
<i>Cyr61</i>	CTGCGCTAAACAACCTCAACGA	GCAGATCCCTTTCAGAGCGG
<i>Ankrd1</i>	GGAACAACGAAAAGCGAGAA	GAAACCTCGGCACATCCACA
<i>Lats2</i>	GGACCCAGGAATGAGCAG	CCCTCGTAGTTTGCACCACC
<i>Dlg1</i>	CGAAGAGTACGTCGTTTTGA	TCTCCAAAGCGGAAGTTTCAGT
<i>Dlg5</i>	CTTTTCCAACGACTCCATTCTC	AGAGAGGTACAGTCCACTTTCTG
<i>Rela</i>	AGATACCACCAAGACCCACC	GGTGACCAGGGAGATTCGAA
<i>Il25</i>	ACAGGGACTTGAATCGGGTC	TGGTAAAGTGGGACGGAGTTG
<i>Il23a</i>	ATGCTGGATTGCAGAGCAGTA	ACGGGGCACATTATTTTTAGTCT
<i>Il12b</i>	TGGTTTGCCATCGTTTTGCTG	ACAGGTGAGGTTCACTGTTTCT
<i>Tslp</i>	ACGGATGGGGCTAACTTACAA	AGTCTCGATTTGCTCGAACT
<i>Camp</i>	GCTGTGGCGGTCACTATCAC	TGTCTAGGGACTGCTGGTTGA
<i>Defb1</i>	AGGTGTTGGCATTCTACAAG	GCTTATCTGGTTTACAGGTTCCC

**Supplementary Table 3.** Primers Used for Identifying MIR31 Target Genes

Gene	Forward Primer 5'–3'	Reverse Primer 5'–3'
<i>Dkk1</i>	GCGCTCGAGTGGGCTTGAATTTGGTAT	TTAGCGGCCGCTCCCGACTATCCTGTGA
<i>Gsk3β</i>	TTAGCGGCCGCTCAGTTTCACAGGGTAT	GCGCTCGAGACAAAGGCATTCAAGTAG
<i>Axin1</i>	GCCTCGAGTCAGTCAGGTGGACAGCC	TAGCGGCCGCACACGGACACTTGAAGG
<i>Lats2</i>	GCGCTCGAGGTACAGAGACCGCTTATCT	ATAGCGGCCGCTTACATTTGCCTCCCGAAGA
<i>Dlg1</i>	GCGCTCGAGGAACAGTCTGGGCCATTACAT	ATAGCGGCCGCTTGCCTCAAGGTCCTAAAT
<i>Dlg5</i>	GCGCTCGAGATAGCCAGCCAGCAGAGGT	ATAGCGGCCGCCAAGGAGGCAGGAGAAAGG
<i>Il6st</i>	GCGCTCGAGGAGTACAGAAGGGCAGAGCA	ATAGCGGCCGCTGAAGCCACTCGTCTTAGC
<i>Il7r</i>	GCGCTCGAGTTCTATTTCTCTCACAA	ATAGCGGCCGCTCATCCCTATAGCCACTTAA
<i>Il17ra</i>	GCGCTCGAGGAAAGATGTGAGGGTAGTGG	ATAGCGGCCGCAAGAAATAGAGCTGGGAAA